AMERICAN SOCIETY FOR MICROBIOLOGY | Journal of Virology®

VIRUS-CELL INTERACTIONS

Targeting Doublecortin-Like Kinase 1 (DCLK1)-Regulated SARS-CoV-2 Pathogenesis in COVID-19

Ram Babu Undi,[a,b] Jason L. Larabee,[c] Adrian Filiberti,[a,b,g] Susanna Ulahannan,[b,h] Sheeja Aravindan,[b] Edana Stroberg,[d] Lisa M. Barton,[d] Eric J. Duval,[d] Sanjay Mukhopadhyay,[e] James C. Henthorn,[i] Darrin Akins,[c] Courtney W. Houchen,[b,f,g,j] Mark M. Huycke,[a,b] Naushad Ali[b,f,g,j]

[a]Department of Radiation Oncology, University of Oklahoma Health Sciences Center, Oklahoma City, Oklahoma, USA
[b]Peggy and Charles Stephenson Cancer Center, University of Oklahoma Health Sciences Center, Oklahoma City, Oklahoma, USA
[c]Department of Microbiology and Immunology, University of Oklahoma Health Sciences Center, Oklahoma City, Oklahoma, USA
[d]Office of the Chief Medical Examiner-Central Division, Oklahoma City, Oklahoma, USA
[e]Department of Pathology, Cleveland Clinic, Cleveland, Ohio, USA
[f]Department of Internal Medicine, University of Oklahoma Health Sciences Center, Oklahoma City, Oklahoma, USA
[g]Digestive Diseases and Nutrition, University of Oklahoma Health Sciences Center, Oklahoma City, Oklahoma, USA
[h]Department of Hematology/Oncology, University of Oklahoma Health Sciences Center, Oklahoma City, Oklahoma, USA
[i]Department of Cell Biology, Flow Cytometry Core Lab, University of Oklahoma Health Sciences Center, Oklahoma City, Oklahoma, USA
[j]Department of Veterans Affairs Medical Center, Oklahoma City, Oklahoma, USA

ABSTRACT Host factors play critical roles in SARS-CoV-2 infection-associated pathology and the severity of COVID-19. In this study, we systematically analyzed the roles of SARS-CoV-2-induced host factors, doublecortin-like kinase 1 (DCLK1), and S100A9 in viral pathogenesis. In autopsied subjects with COVID-19 and pre-existing chronic liver disease, we observed high levels of DCLK1 and S100A9 expression and immunosuppressive ($DCLK1^+S100A9^+CD206^+$) M2-like macrophages and N2-like neutrophils in lungs and livers. DCLK1 and S100A9 expression were rarely observed in normal controls, COVID-19-negative subjects with chronic lung disease, or COVID-19 subjects without chronic liver disease. In hospitalized patients with COVID-19, we detected 2 to 3-fold increased levels of circulating $DCLK1^+S100A9^+$ mononuclear cells that correlated with disease severity. We validated the SARS-CoV-2-dependent generation of these double-positive immune cells in coculture. SARS-CoV-2-induced DCLK1 expression correlated with the activation of β-catenin, a known regulator of the DCLK1 promoter. Gain and loss of function studies showed that DCLK1 kinase amplified live virus production and promoted cytokine, chemokine, and growth factor secretion by peripheral blood mononuclear cells. Inhibition of DCLK1 kinase blocked pro-inflammatory caspase-1/interleukin-1β signaling in infected cells. Treatment of SARS-CoV-2-infected cells with inhibitors of DCLK1 kinase and S100A9 normalized cytokine/chemokine profiles and attenuated DCLK1 expression and β-catenin activation. In conclusion, we report previously unidentified roles of DCLK1 in augmenting SARS-CoV-2 viremia, inflammatory cytokine expression, and dysregulation of immune cells involved in innate immunity. DCLK1 could be a potential therapeutic target for COVID-19, especially in patients with underlying comorbid diseases associated with DCLK1 expression.

IMPORTANCE High mortality in COVID-19 is associated with underlying comorbidities such as chronic liver diseases. Successful treatment of severe/critical COVID-19 remains challenging. Herein, we report a targetable host factor, DCLK1, that amplifies SARS-CoV-2 production, cytokine secretion, and inflammatory pathways via activation of β-catenin (p65)/DCLK1/S100A9/NF-κB signaling. Furthermore, we observed in the lung, liver, and blood an increased prevalence of immune cells coexpressing DCLK1 and S100A9, a myeloid-derived proinflammatory protein. These cells were associated with increased disease severity in COVID-19 patients. Finally, we used a novel small-molecule inhibitor of DCLK1

Editor Kanta Subbarao, The Peter Doherty Institute for Infection and Immunity

Address correspondence to Naushad Ali, Naushad-ali@ouhsc.edu.

The authors declare no conflict of interest.

Received 22 June 2022
Accepted 13 July 2022
Published 9 August 2022

kinase (DCLK1-IN-1) and S100A9 inhibitor (tasquinimod) to decrease virus production *in vitro* and normalize hyperinflammatory responses known to contribute to disease severity in COVID-19.

KEYWORDS COVID-19, DDCLK1, immune response, S100A9, SARS-CoV-2, treatment, virus replication, inflammation

The coronavirus disease 2019 (COVID-19) pandemic represents the most significant global public health crisis (1). The severe acute respiratory coronavirus 2 (SARS-CoV-2) and its variants of concern (e.g., delta and omicron) were causative agents of this pandemic (2). Although many people who contracted COVID-19 were asymptomatic or presented with only mild symptoms (80%), in a minority of cases the infection can rapidly progress to hypoxia and acute respiratory distress syndrome. This is especially true for elderly patients and those with underlying comorbid medical conditions (3, 4). Deep immune profiling of COVID-19 patients reveals heterogeneous immune responses (5). A characteristic cytokine storm is also noted in severely ill patients (6). Although the lung is the primary organ affected in severe disease, tissue- and organotropism have also been documented (7). Among comorbid factors for COVID-19, preexisting chronic liver disease (CLD) is associated with poor outcomes and high mortality rates (8, 9).

The angiotensin-converting enzyme type 2 (ACE2) protein is the main viral receptor for SARS-CoV-2. In adults, this membrane-bound peptidase is normally expressed on type II pneumocytes, endothelial cells, arterial smooth muscle cells, cholangiocytes, and intestinal epithelial cells (10). In contrast, ACE2 is rarely expressed by hepatocytes in healthy livers (10). However, ACE2 is strongly induced by hepatocytes in livers with fibrosis, cirrhosis, and immune activation (11, 12). As a result, in CLD, this organ, in addition to the lung, becomes a potential site for SARS-CoV-2 infection. The potential for increased pathophysiology may occur as liver cells are infected by SARS-CoV-2. However, underlying mechanisms for decompensation in persons with COVID-19 and CLD remain poorly understood.

We previously showed that doublecortin-like kinase 1 (DCLK1) is induced by tissue injury and inflammation in the liver, lung, and gastrointestinal tract (13, 14). DCLK1 is a multifunctional protein known for its involvement in clonogenicity, stemness, and tumorigenesis (15–18). It catalyzes tubulin polymerization that facilitates intracellular molecular transport and the replication of several viruses (e.g., adenoviruses, herpesviruses, and influenza viruses) (19). DCLK1 also contains a kinase domain that phosphorylates multiple substrates, including the Spen family transcriptional repressor and cyclin-dependent kinase 11B (20). Our previous work showed that DCLK1 overexpression enhances the replication of the hepatitis C virus, a positive-strand RNA virus, by regulating microtubule dynamics (15, 21, 22). In contrast, downregulating DCLK1 inhibited hepatitis C virus replication and slowed the growth of hepatocellular carcinoma (23). In one clinical trial, colchicine, a drug that inhibits microtubule polymerization, was shown to lower hospitalization rates for COVID-19 patients (24).

Another potential role for DCLK1 in COVID-19 might occur through its regulation of the proinflammatory myeloid-derived S100A9 protein. DCLK1 and S100A9 are each response elements to tissue injury and inflammation. When overexpressed, DCLK1 upregulates S100A9 whereas DCLK1 knockdown reduces the expression of S100A9 (12). During inflammation, S100A9 is expressed by many epithelial and immune cells and is a promising biomarker for severe COVID-19 (25, 26). This protein forms complexes with S100A8 that are termed calprotectin, and these complexes can activate nuclear factor (NF)-κB via multiple surface receptors (e.g., Toll-like receptor [TLR] 4), receptor for advanced glycation end products, and a cluster of differentiation (CD) 33. This induces interleukin (IL)-1β, IL-6, tumor necrosis factor (TNF)-α, IL-10, and inducible nitric oxide synthase (27, 28). Although the expression of DCLK1, including alternative splicing and posttranslational processing, is poorly understood, it is generally accepted that β-catenin and nuclear factor (NF)-κB regulate DCLK1 promoters (29–31). In

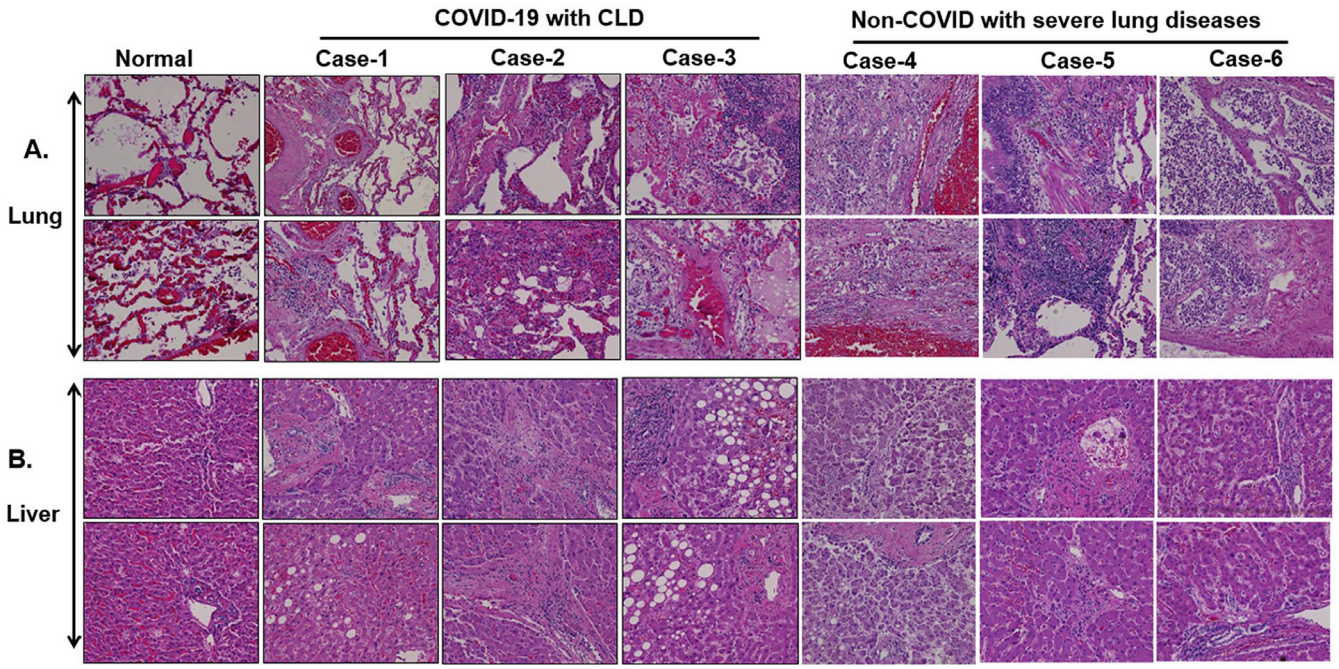

FIG 1 H&E staining representative of the autopsied lung (A) and liver (B) tissues from COVID-19 and non-COVID-19 lung disease cases. Photomicrographs show two separate areas for each individual. Histopathologic interpretations are summarized in Table 1. Magnification: 20×.

addition, S100A9 is also regulated via NF-κB, likely through feed-forward mechanisms. These observations provide additional reasons to investigate the role of these proteins in the hyperinflammatory milieu of severe COVID-19. This is especially relevant for patients with CLD as both proteins are elevated under these conditions (12, 32).

Together, these observations provide a strong rationale for investigating the role of DCLK1 in SARS-CoV-2 infection for patients with CLD. Herein, we identified the liver as an important site of SARS-CoV-2 replication in persons with CLD due to pre-existing expression of DCLK1. In addition, we show that DCLK1 can modulate SARS-CoV-2 production, cytokine induction, and viral immune evasion. Finally, we show that small molecule inhibitors of DCLK1 and S100A9 limit viral production, DCLK1 expression, and hyperinflammation. These studies identify DCLK1 as a novel host target for its potential therapeutic significance in severe COVID-19, especially in the context of CLD.

RESULTS

DCLK1 was expressed at the site of SARS-CoV-2 infection in the lung and liver of COVID-19 patients. We analyzed the lung and liver tissues of individuals (n = 11) who were autopsied by the Oklahoma City Office of Chief Medical Examiner (OCME) during the early pandemic. Based on detailed autopsy investigations and hematoxylin and eosin (H&E) staining results (33), the subjects were identified as (i) COVID-19 with CLD (Cases 1, 2, and 3); (ii) non-COVID-19 (SARS-CoV-2-negative) with severe lung disease but no liver disease (Cases 4, 5, and 6); and (iii) COVID-19 with mild liver disease or histologically normal liver (Cases 7, 8, and 9). For comparison, we used as controls the autopsies of two persons (N-1 and N-2) who did not have COVID-19 or lung or liver pathology but died from drowning or cardiomyopathy. The clinical findings and representative photomicrographs of the lung and liver histology and histopathology for these cases and controls are shown in Fig. 1 and summarized in Table 1. Immunofluorescence staining of tissues for the COVID-19 cases with CLD (Cases 1, 2, and 3) showed strong patchy staining for ACE2, Spike protein of SARS-CoV-2, and DCLK1, in both lungs (Fig. 2A, only Case 1 is shown) and liver (Fig. 2B). The COVID-19 cases with mild or no liver steatosis (Cases 7, 8, and 9) showed absent to moderate staining for ACE2, Spike, and DCLK1 in lung and rare to no staining in the liver. In contrast, the lungs and livers from normal (N-1 and N-2) and non-COVID-19 cases with pre-existing lung disease (Cases 4, 5, and 6)

TABLE 1 Summary of autopsied subjects with immunohistochemical (IHC) findings for lung and liver[a]

				Lung IHC					Liver IHC			
Autopsied subjects	**Age (y)**	**Gender**	**Lung histopathology**	**ACE2**	**Spike**	**DCLK1**	**S100A9**	**Liver histopathology**	**ACE2**	**Spike**	**DCLK1**	**S100A9**
Normal lung and liver												
Normal (N)-1	22	F	Normal	+	−	+	+	Normal	−	−	+/−	+
Normal (N)-2	28	F	Normal	+	−	+	+	Normal	−	−	−	+
COVID-19 with chronic liver disease												
Case-1	77	M	Diffuse alveolar damage	+++	+++	+++	+++	Pre-existing centrilobular steatosis and portal inflammation with focal necrosis and acute inflammation	+++	+++	++	+++
Case-2	42	M	Acute broncho-pneumonia with bilateral consolidations	+++	+++	+++	+++	Pre-existing micronodules with bridging fibrosis and chronic inflammation of portal tracts	++	+++	++	+++
Case-3	26	M	Diffuse alveolar damage	+	+++	+++	+++	Pre-existing advanced steatosis with microthrombi in portal arteries	++	+++	+++	+++
Non-COVID-19 with severe lung disease												
Case-4	53	M	Diffuse alveolar damage due to exposure to toxic fumes	ND	ND	+	+	Pre-existing mild steatosis with mild chronic inflammation of portal tracts	ND	ND	−	+/−
Case-5	47	M	Aspiration pneumonia due to drowning	ND	ND	+	+	Pre-existing chronic inflammation of portal tracts	ND	ND	−	+/−
Case-6	74	M	Diffuse alveolar damage due to necrotizing bacterial	ND	ND	−	−	Pre-existing chronic inflammation of portal tracts	ND	ND	+	+
COVID-19 with normal or mild liver disease												
Case-7	53	M	Acute bacterial pneumonia with diffuse alveolar damage, intraalveolar edema, and microthrombi	++	++	++	+	Normal	+/−	+/−	−	+
Case-8	36	M	Diffuse alveolar damage with microthrombi	+	+	+/−	+++	Pre-existing mild steatosis	−	−	−	+
Case-9	52	F	Early changes of viral pneumonia	−	+	−	++	Pre-existing mild steatosis	−	−	−	+

[a]Staining was assessed as being absent (−), rare (+/−), weak (+), moderate (++), or strong (+++).

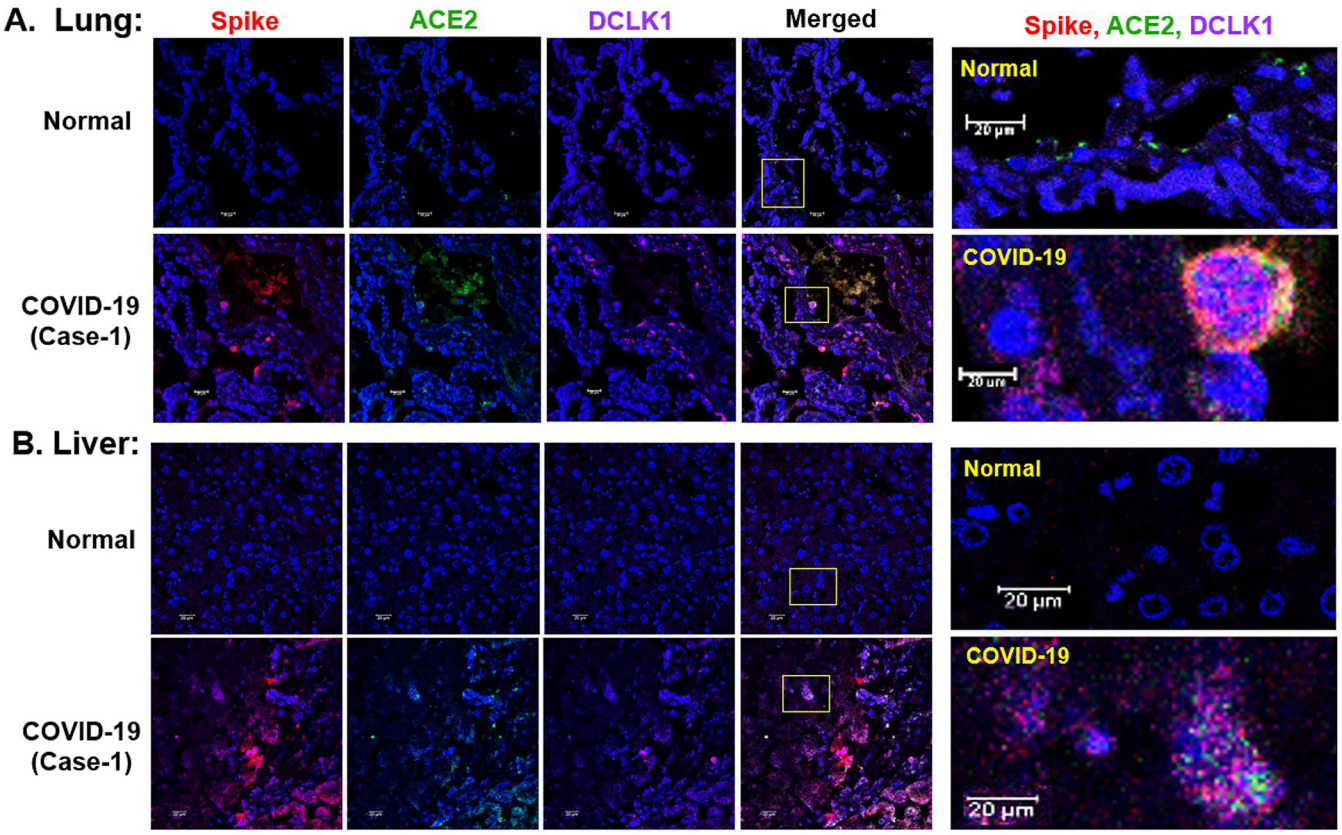

FIG 2 DCLK1 expression and SARS-CoV-2 infection in lung and liver for a representative COVID-19 case and normal control. (A) Lung tissues from one COVID-19 autopsy and a normal control were immunostained for SARS-CoV-2 Spike (red), ACE2 (green), and DCLK1 (magenta) and imaged by confocal microscopy. Cellular staining patterns are highlighted (yellow boxes; right, highlighted). Intracellular Spike is seen at sites of active SARS-CoV-2 infection. (B) Representative liver biopsy specimens from the same case and normal control as in (A) showing Spike (red), ACE2 (green), and DCLK1 (magenta) at sites of infection. Nuclear stain, blue. Scale, 20 μm.

showed minimal to no staining for ACE2 and DCLK1 (Figs. 1 and 2 and Table 1). These results indicated that individuals with CLD who succumbed to SARS-CoV-2 infection had markedly increased expression for ACE2, Spike, and DCLK1 in lung and liver compared to COVID-19 cases without CLD and non-COVID-19 controls.

M2-like macrophages coexpressed DCLK1 and S100A9 and correlated with disease severity. S100A9 plays important role in the dysregulation of the innate immune system in many diseases, including COVID-19 (28, 34, 35). It is also positively regulated by DCLK1 (12). We observed strong S100A9 staining in both epithelial, alveolar, and sinusoidal cells during initial investigations, (Cases 1, 2, and 3; Table 1), This observation led us to determine DCLK1 and S100A9 status in immune cells. We co-stained for DCLK1, S100A9, and macrophage markers. The lungs of COVID-19 cases with CLD showed extensive co-staining for DCLK1 and S100A9 in CD206$^+$ M2-like polarized macrophages (Fig. 3A and B). These triple-positive cells (DCLK1$^+$S100A9$^+$CD206$^+$) were primarily located in alveolar spaces and adjacent to interstitial compartments (see Video 1 for relative positions of these markers within the cells). Quantitative evaluation of 5 areas within stained lung tissues of each individual revealed that COVID-19 cases with CLD had 4 to 5-fold increased numbers of triple-positive macrophages compared with non-COVID-19 cases with lung disease (Cases 4, 5, 6; Fig. 3C). Similarly, high levels of DCLK1$^+$S100A9$^+$CD206$^+$ macrophages were also observed in the livers of Cases 1 to 3 compared to Cases 4 to 6. (Fig. 3D to F; see Video 2 for marker locations). However, staining intensity was minimal, and numbers of triple-positive cells were rare in lungs and livers of normal (N-1 and N-2), non-COVID-19 subjects (Cases 4 to 6), and COVID-19 subjects without CLD (Cases 7 to 9). For the latter group, S100A9$^+$/CD68$^+$ M1-like macrophages were observed instead of triple-positive cells (unpublished data). The

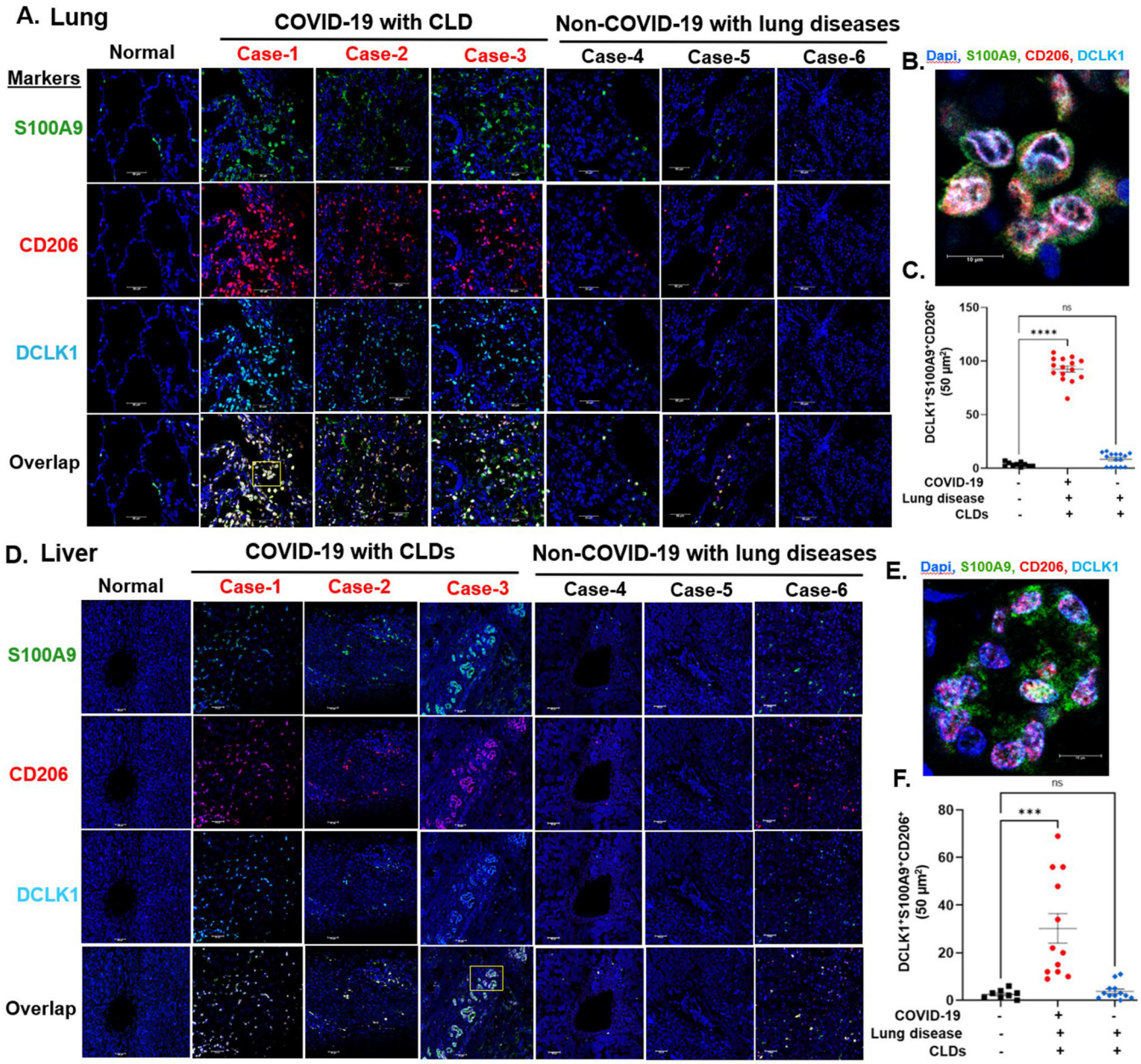

FIG 3 DCLK1 and S100A9 coexpressing immunosuppressive M2 macrophages ($CD206^+$) extensively accumulate in the lungs of COVID-19 individuals. (A) Confocal microscopy of the lung from autopsied subjects with COVID-19, non-COVID-19 with lung diseases, and normal case controls (left) after costaining for S100A9 (green), CD206 (red), DCLK1 (cyan), and nucleus (blue); scale, 20 μm. (B) Boxed yellow areas (Case-1) are highlighted at the bottom. (C) Quantitative evaluation of $DCLK1^+S100A9^+CD206^+$ macrophages from the stained lungs (50 μm^2/area), 15 dots represent 3 cases, and 5 sites were evaluated for each case. (D) Corresponding liver of individuals shown in (A) were costained for S100A9 (green), DCLK1 (cyan), CD206 (red), and nucleus (blue). The images were visualized by confocal microscopy. (E) The yellow boxed area (Case-3) is highlighted to reveal triple-positive ($DCLK1^+S100A9^+CD206^+$) M2 macrophages in the liver. Magnification, 60×. (F) Quantitation of $DCLK1^+S100A9^+CD206^+$ macrophages from stained livers (50 μm^2/area), 4 sites in the stained slides were evaluated for each case. Twelve dots (e.g., COVID-19 or non-COVID-19) represent 3 cases in each group as shown in (D). For two normal cases, 8 dots represent 4 sites for each one on the stained slides.

triple-positive cells had kidney-shaped nuclei that were morphologically compatible with macrophages (Fig. 3B). In addition, a small number of triple-positive N2-like neutrophils were also noted, which were defined by their characteristics of hypersegmented nuclei and CD206 expression (36). These findings suggested that increased numbers of triple-positive $DCLK1^+S100A9^+CD206^+$ M2-like macrophages and N2-like neutrophils were common in lung and liver of COVID-19 subjects with CLD.

We next wanted to determine whether triple-positive immune cells also occurred as circulating cells in the blood of COVID-19 patients. Because peripheral blood

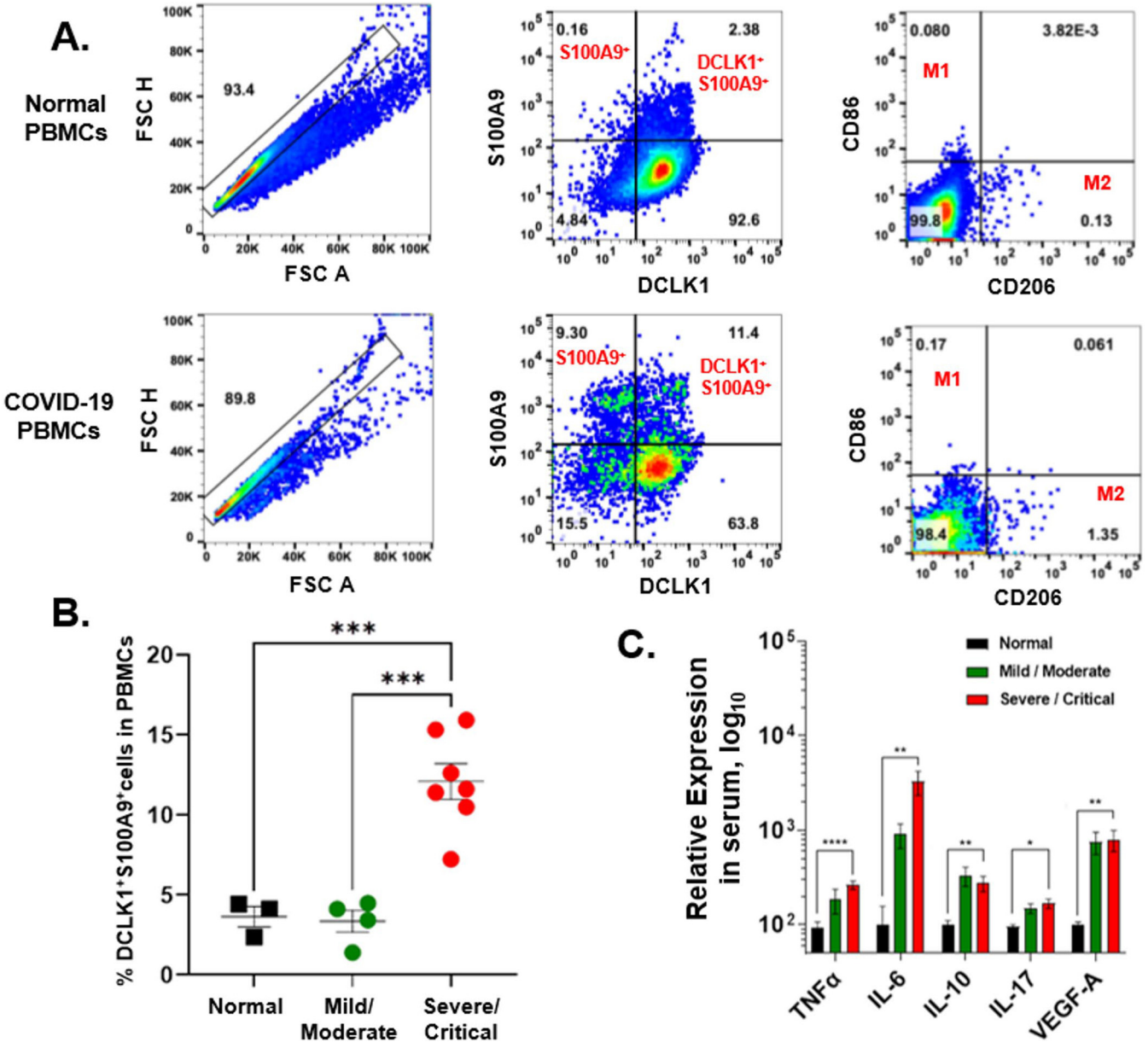

FIG 4 COVID-19 patients exhibited high levels of DCLK1 and S100A9 coexpressing mononuclear cells in the blood that correlated with the severity of COVID-19. (A) Flow cytometry of PBMCs from normal adults and COVID-19 patients for DCLK1, S100A9, and M1 (CD86) and M2 (CD206) macrophage markers. Cells were stained with antibody conjugates or corresponding isotype control IgG-conjugates (negative controls used for gating). (B) The percentage of DCLK1$^+$S100A9$^+$ cells in PBMC populations from seven severe/critical and four mild/moderate COVID-19 patients and three normal healthy adults. (C) Sera from 3 normal (black bar) and 17 COVID-19 inpatients (6 mild/moderate [green bar] and 11 severe/critical [red bar]) were analyzed for cytokines. Cytokine levels were arbitrarily set at 100 for normal and compared with patients' sera.

mononuclear cells (PBMCs) were not available for postmortem cases, we analyzed PBMCs from the blood of 11 hospitalized COVID-19 patients (4 with mild-to-moderate disease and 7 severe/critical disease) and the blood of 3 normal healthy adults. We note that these patients were hospitalized in 2020 and received standard of care for COVID-19 at that time (e.g., remdesivir, steroids, and/or convalescent plasma). PBMCs of severe COVID-19 patients had 3 to 4-fold greater numbers of circulating DCLK1$^+$S100A9$^+$ mononuclear cells compared to PBMCs from normal or patients with mild-to-moderate COVID-19 (Fig. 4A and B). Few of these cells, however, had CD86$^+$ M1-like or CD206$^+$ M2-like phenotypes indicative of polarized macrophages. Analysis of sera for COVID-19 patients revealed high levels of proinflammatory (TNF-α, IL-6, and IL-17) and anti-inflammatory (IL-10) cytokines, and the

angiogenic factor vascular endothelial growth factor (VEGF)-A compared to normal control sera (Fig. 4C).

DCLK1 and S100A9 inhibitors blocked the production of infectious SARS-CoV-2 particles and inflammatory responses. To further explore the potential role of DCLK1 in SARS-CoV-2 infection, we infected Calu3 cells (a lung adenocarcinoma cell line) and measured the production of infectious virus particles following treatment with a well-characterized small-molecule inhibitor of DCLK1 kinase (DCLK1-IN-1). This inhibitor strongly binds the kinase domain of DCLK1 with high specificity (K_D = 109 nM) (20, 37). A structural analog, DCLK1-NEG, with low binding affinity was used as a negative-control (37). The DCLK1-IN-1 treatment of infected cells showed a strong dose-response reduction in intracellular viral proteins (nucleocapsid and Spike) (Fig. 5A, lanes 4 to 6) compared to untreated control (lane 1). There was an approximate 65% and 95% loss of these proteins at 5 μM and 10 μM, respectively. DCLK1 protein levels were not significantly affected by treatment. These results suggested that the kinase activity of DCLK1 promoted viral replication. Tissue culture infectious dose 50 ($TCID_{50}$) analysis of SARS-CoV-2 infectious particles in culture supernatants from treated and untreated samples showed a 4-fold and 10-fold decrease in infectivity at 5 μM and 10 μM DCLK1-IN-1, respectively (Fig. 5B). The negative-control DCLK1-NEG at 5.0 μM did not reduce Spike (Fig. 5C), suggesting that reductions in SARS-CoV-2 viral particle production by DCLK1-IN-1 were specifically due to inhibition of kinase activity. We confirmed DCLK1-IN-1-mediated downregulation of Spike using immunofluorescence (Fig. 5D, bottom; Fig. 5E, highlighted at the bottom). It was notable that many cells with little to no staining for Spike showed intense staining for DCLK1 implying potential paracrine signaling between cells.

To further investigate the mechanisms of DCLK1 regulation of SARS-CoV-2 pathogenesis, we next treated infected Calu3 cells with DCLK1-IN-1 alone or in combination with tasquinimod (TasQ), an S100A9 inhibitor. SARS-CoV-2 induction of DCLK1 was accompanied by activation of the full-length (p92) and a smaller form (p65) of active β-catenin (Fig. 5F, lane 2 compared with lane 1). An anti-active β-catenin monoclonal antibody that specifically recognizes the unphosphorylated N terminus motif was used for detecting these bands (38). DCLK1-IN-1 plus tasquinimod attenuated activate β-catenin(p65) and DCLK1 (Fig. 5F, lane 5), suggesting induction of DCLK1/S100A9 through β-catenin (p65) by SARS-CoV-2. Similarly, viral infection increased p45 (unprocessed) and p20 (active) forms of caspase 1 (Fig. 5F, lane 2). This correlated with high levels of pro-IL-1β (p35) and active (p17) IL-1β (a downstream target of caspase 1) and granulocyte-macrophage colony-stimulating factor (GM-CSF). DCLK1-IN-1, tasquinimod, and combined treatments downregulated active forms of caspase 1 and IL-1β (Fig. 5F, lanes 3, 4, and 5). Intracellular GM-CSF and S100A9 levels were not affected by these inhibitors. We next determined whether interferon (IFN) β as part of the cellular antiviral response to SARS-CoV-2 infection was modulated by inhibiting the kinase activity of DCLK1 or S100A9. IFN-β produced by infected cells was normalized when treated with the inhibitors (Fig. 5G). These findings suggested that targeting the kinase activity of DCLK1 and/or S100A9 may be useful to limit inflammation and bolster antiviral cellular responses to SARS-CoV-2.

SARS-CoV-2 infection induced DCLK1$^+$S100A9$^+$ mononuclear immune cells and M1-like macrophages. We next determined whether the association of triple-positive DCLK1$^+$S100A9$^+$CD206$^+$ macrophages with severe/critical SARS-CoV-2 infection was due to the exposure of immune cells to viral-infected lung or liver cells. Infected Calu3 cells were incubated with normal human PBMCs in a dual-chamber system that prevented cellular contact but allowed for the free diffusion of soluble factors. When cultured alone, live singlet PBMCs gated for side scatter (SSC)-high and SSC-low morphologies showed few DCLK1$^+$S100A9$^+$ mononuclear cells and few M1-like (CD86$^+$) or M2-like (CD206$^+$) macrophages (Fig. 6A, top). However, compared to uninfected controls, an increase in DCLK1$^+$S100A9$^+$ SSC-high cells was observed when PBMCs were exposed to SARS-CoV-2-infected Calu-3 cells (Fig. 6A, bottom left). These SSC-high cells were predominantly negative for CD86 and CD206 markers, suggesting they were not

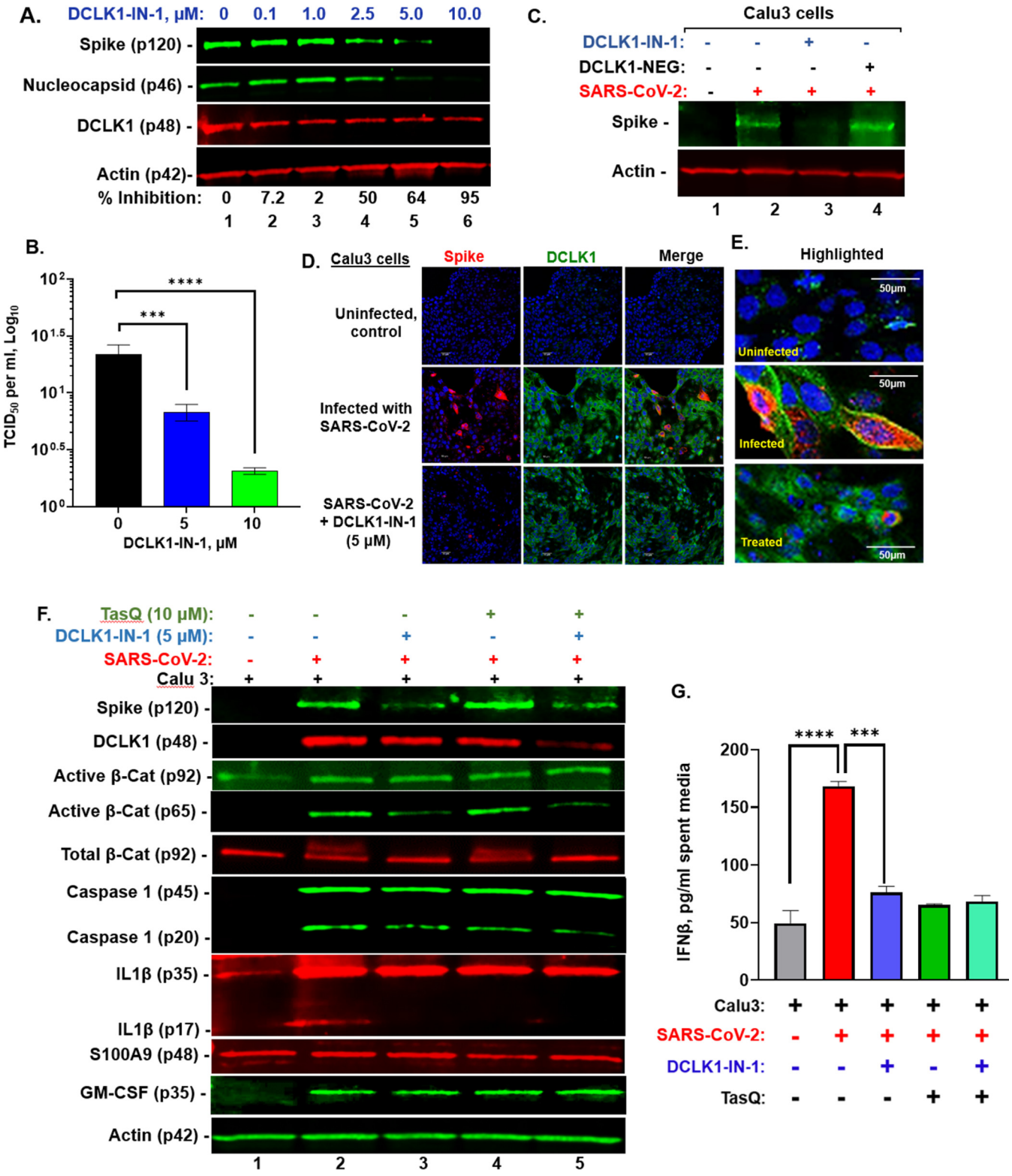

FIG 5 DCLK1 kinase facilitates the production of infectious SARS-CoV-2 particles and inflammatory signaling. (A) Calu3 lung cells infected with SARS-CoV-2 (multiplicity of infection = 1) were treated with DCLK1 kinase inhibitor (DCLK1-IN-1). Spike, nucleocapsid, and DCLK1 were detected by Western blotting with replicates performed. (B) Titers of SARS-CoV-2 virions in spent media at 0, 5, and 10 μM DCLK1-INH-1 were assessed by $TCID_{50}$. $P < 0.0005$ (***); $P < 0.00005$ (****). (C) Comparison of Spike after treatment of infected Calu3 cells with 5 μM DCLK1-IN-1 (lane 3) or DCLK1-NEG (small molecule negative-control, lane 4). (D) Confocal microscopy for DCLK1 (green) and Spike (red) in uninfected Calu3 cells (upper), infected but untreated cells (middle), and inhibitor-treated cells (lower). (E) Magnified cells show patterns of Spike (red) and DCLK1 (green) expression in uninfected, infected, and inhibitor-treated Calu3 cells with infection. (F) Western blots of total cell lysates from uninfected (lane 1) and infected (lane 2) Calu3 cells. Infected cells were treated with

(Continued on next page)

M1 or M2 polarized macrophages (unpublished data). Finally, for PBMCs exposed to infected Calu3 cells, SSC-low cells representing lymphocytes and monocytes showed little to no change in the small proportions of M1-like and M2-like cells compared to untreated controls (Fig. 6A, lower right). These results showed that soluble factors from SARS-CoV-2-infected cells generated DCLK1$^+$S100A9$^+$ cells although did not polarize blood monocytes into M1-like or M2-like macrophages.

To determine the potential role of cell-cell contact on induction of DCLK1$^+$S100A9$^+$CD206$^+$ mononuclear immune cells, a similar analysis was performed using PBMCs and SARS-CoV-2-infected Calu3 cells in mixed culture. Again, a substantial increase in DCLK1$^+$S100A9$^+$ cells was observed in SSC-high populations (Fig. 6B, middle). SSC-low cells showed an increase in their proportions of M1-like, but not M2-like cells (Fig. 6B, right). We tested secreted cytokine/chemokine levels in both coculture formats (transwell and mixed) using spent media. Supernatants showed marked increases in TNF-α, IFN-β, IL-1β, IL-6, and IL-10 for infected cultures compared to uninfected controls in the transwell system (Fig. 6C). In the mixed cocultures that allowed infected cell-immune cell interactions, similar increases were observed in these cytokines along with modest increases in M-CSF, GM-CSF, IFN-α, and IFN-γ (Fig. 6D). The C-C motif chemokine ligand 2 (CCL2/MCP-1) was downregulated in mixed culture although increased levels have been reported for patients with severe/critical COVID-19 (39, 40). Because NF-κB is involved in macrophage polarization to the M1-like phenotype, and the upregulation of inflammatory cytokines, we performed Western blots of lysates for the activated form of NF-κB (p-NF-κB(65)^{Ser536}) and total NF-κB in infected and uninfected Calu3 cells cultured with PBMCs (Fig. 6E). While total NF-κB was maintained at basal levels, infection increased the activated form of NF-κB. Because NF-κB is activated by S100A9/TLR4 pathways in macrophages (41), increases in activated NF-κB (Fig. 6E, lane 2) were likely due to polarized macrophages. The upregulation of IFN-γ and other chemokines along with increased proportions of M1-like macrophages in mixed culture suggests that SARS-CoV-2-infected cells induce a strong proinflammatory Th1 response as typically seen in severe COVID-19 (42).

SARS-CoV-2-infected human hepatocytes expressed DCLK1 and S100A9 and generated a proinflammatory immune response. Persons with CLD have a higher risk for fatal outcomes with COVID-19 compared to those without liver disease (8, 9). Both DCLK1 and S100A9 are highly expressed in CLD, including fatty liver, cirrhosis, and hepatocellular carcinoma. To determine whether SARS-CoV-2-infected cells with high DCLK1 expression have increased viral replication, we used primary human hepatocytes (PHHs) cultured cells on thin Matrigel layers to retain plasticity and lineages (15, 23). The ACE2 viral receptor was highly expressed under these conditions (Fig. 7A, upper). Cells infected with SARS-CoV-2 at a multiplicity of infection (MOI) of 1 were markedly positive for Spike (Fig. 7A, lower). Viral infection also strongly induced DCLK1 and S100A9 (Fig. 7B). As observed with the Calu3 cells and in livers from COVID-19 cases with CLD, ACE2-expressing hepatocytes were susceptible to SARS-CoV-2 and infection was associated with DCLK1 and S100A9 expression.

As reported by others (43), we next confirmed the susceptibility of Huh7 human hepatoma cells to infection with SARS-CoV-2. Similar to experiments using PHHs, these cells strongly induced DCLK1 and S100A9 when infected (Fig. 7C). SARS-CoV-2 also led to the expression of immunomodulatory cytokines (GM-CSF and M-CSF) and M-CSF-R/CD115 receptors. These cofactors help drive proinflammatory signaling and macrophage recruitment/polarization. Mixing SARS-CoV-2-infected Huh7 cells with normal human PBMCs strongly induced a CD68$^+$/CD86$^+$ M1-like macrophage phenotype with a corresponding loss of CD206$^+$/Arg-1$^+$ M2-like markers (Fig. 7D). Thus, SARS-CoV-2 infection of DCLK1-expressing hepatoma cells promoted an M1-like polarization of

FIG 5 Legend (Continued)
DCLK1-IN-1 (5 μM, lane 3), tasquinimod (TasQ,10 μM, lane 4), or both (lane 5). (G) Spent media (from the above-described experiment) were assayed for IFN-β (indicates antiviral responses) for infected Calu3 cells (colored bars) compared to uninfected controls (gray). Infected cells were treated with DCLK1-IN-1 (blue) or tasquinimod (green) or both (cyan). Data are mean $\pm$ SEM.

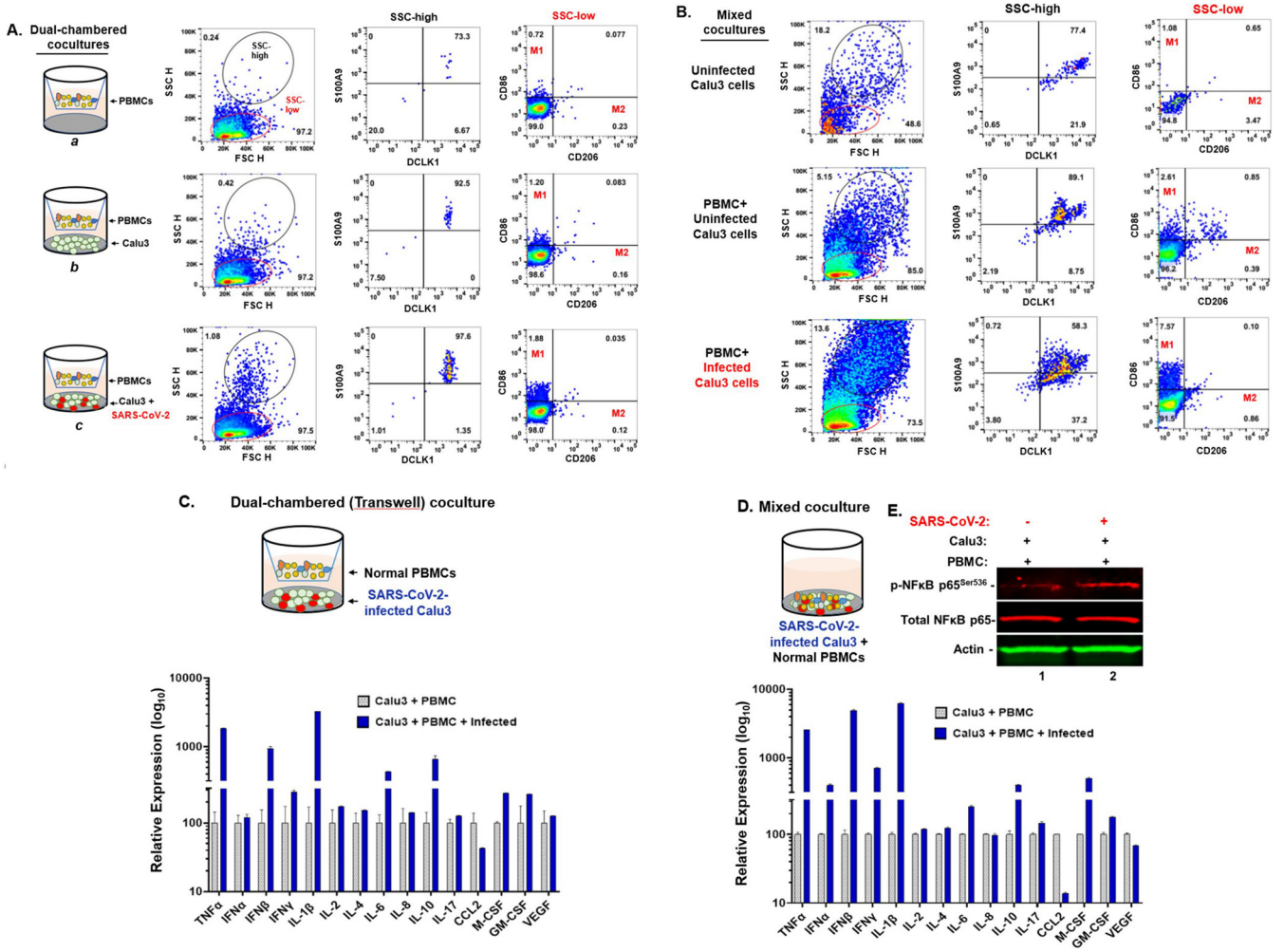

FIG 6 SARS-CoV-2-infected cells induce DCLK1$^+$S100A9$^+$ monocytes and M1-like macrophages in normal human PBMCs. (A) Normal human PBMCs were cultured with uninfected or SARS-CoV-2-infected Calu3 cells for 48 h in a dual-chamber culture system (representative histograms shown). PBMCs were cultured in upper inserts while uninfected or infected Calu3 cells were in lower chambers. PBMCs were analyzed by multicolor flow cytometry after staining with antibody-fluorophore conjugates. Respective isotype IgG-fluorophore conjugates were used as negative controls for gating (not shown). Live cells with large (SSC-high, black circles) or low (SSC-low, red circles) granular morphology were analyzed. Cells with large granular morphology were predominantly DCLK1$^+$S100A9$^+$ (middle). Low granularity cells (predominantly monocytes and lymphocytes) were analyzed for CD86$^+$ (M1-like) and CD206$^+$ (M2-like) polarized macrophages (right) with quadrants defined by isotype-IgG-fluorophore conjugates (not shown). (B) Normal human PBMCs cocultured with infected or uninfected Calu3 cells in the same chamber (mixed cocultures) were analyzed by flow cytometry as described in (A). Live large granular cells (SSC-high, black circles, left) were predominantly DCLK1$^+$S100A9$^+$ (middle). Low granularity cells (SSC-low, red circles, left) represent lymphocytes and monocytes. Analysis of these cells showed an increase (approximately 3-fold) in the proportion of CD86$^+$ (M1-like) cells in the mixed cocultures (right bottom) compared to the uninfected control (middle right). Spent media from dual-chamber (C) and mixed (D) cocultures were analyzed for cytokines, chemokines, and growth factors using a Luminex assay kit; samples assayed in duplicate with SEM are shown. (E) Western blot for the total lysates of infected and uninfected mixed cocultures for probing activated NF-κB (p- NF-κB(65))^{Ser536} and total NF-κB.

PBMCs. These findings are consistent with observations that used infected Calu3 cells (Fig. 6B). Infected Huh7 cells also had increased levels of caspase 1 and IL1β (Fig. 7E). Mixed cultures of infected Huh7 cells with PBMCs led to an accumulation of unprocessed (i.e., high molecular weight) caspase 1 (p45 and p42) and pro-IL-1β (p31) at 48 h. This was accompanied by the downregulation of NLRP3. Longer incubations of these cultures were not feasible due to increased cell death over time (Fig. 7G).

DCLK1 amplified SARS-CoV-2 production by liver cells. To test whether DCLK1-overexpressing liver cells generally present in CLD could amplify SARS-CoV-2 production, Huh7 cells were engineered to overexpress N-terminal red fluorescent protein (RFP) tagged human DCLK1 (Huh7-RFP-DCLK1). The biological activities of the expressed RFP-DCLK1 in these cells have been established previously (15, 21). Huh7 cells and Huh7 cells expressing RFP alone (Huh7-RFP) were used as controls. After infection with SARS-CoV-2, the spent media from infected cells were assayed by $TCID_{50}$

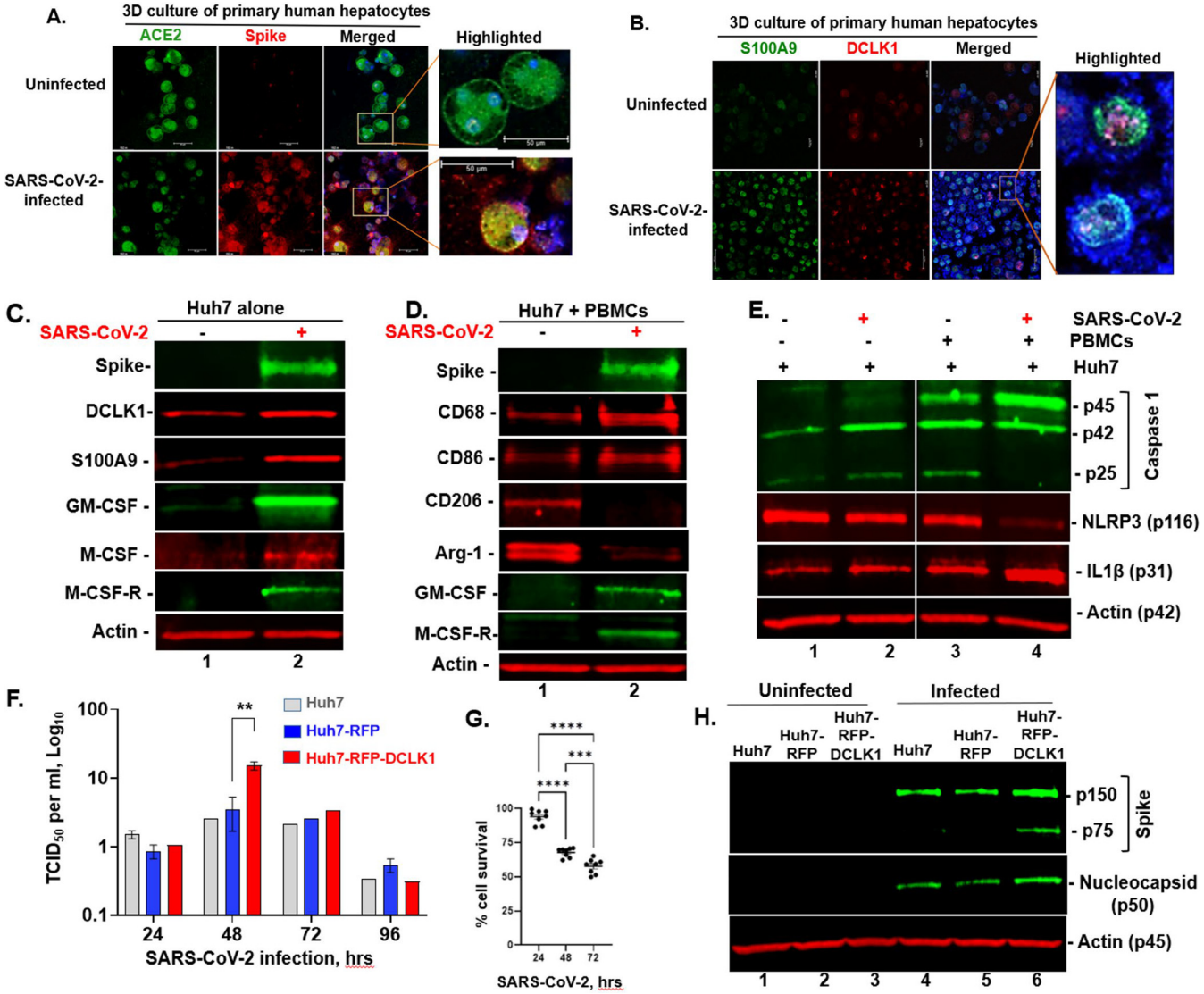

FIG 7 DCLK1-mediated upregulation of SARS-CoV-2 production in the liver promotes viremia, inflammatory response, and immune dysfunction. (A) Primary human hepatocytes (PHHs were cultured on a thin layer of Matrigel for 24 h and infected with SARS-CoV-2). After 72 h, cells were imaged by confocal microscopy for ACE2 (green) and Spike (red). Highlighted (yellow box) cells show a pattern of the cell membrane and intracellular ACE2 expression in the uninfected cells (upper). Lower, infected cells (B) Confocal microscopy of uninfected (upper) and infected (lower) PHHs for S100A9 (green) and DCLK1 (red). Highlighted (right) shows DCLK1^{+}S100A9^{+} PHHs after the viral infection. Intense staining of cellular cytoplasm with Dapi (blue) in infected PHHs is likely due to viral RNA (bottom), which is not present in uninfected cells (upper). (C) Western blot of hepatoma Huh7 cell lysates (lane 1, uninfected; lane 2, infected). (D) Western blots of mixed cocultures of normal human PBMCs with uninfected (lane 1) or SARS-CoV-2-infected (lane 2) Huh7 cells. (E) SARS-CoV-2 downregulates NLRP3 and enhances the intracellular accumulation of unprocessed caspase 1 and IL-1β at an early stage of infection (48 h of infection) in mixed cocultures. Western blots of total lysates from infected or uninfected cultures of Huh7 cells (lanes 1 and 2). Western bot for mixed cocultures of PBMCs and infected (lane 4) or uninfected (lanes 3) Huh7 cells. (F) DCLK1 enhances SARS-CoV-2 production. Huh7, Huh7-RFP (control), and Huh7-RFP-DCLK1 (overexpressing recombinant human DCLK1) cells were infected with SARS-CoV-2 and infectious viral particles in spent media assayed at 24, 48, 72, and 96 h postinfection by $TCID_{50}$ (P = 0.002). (G) Cell survival assay for Huh7-RFP-DCLK1 cells at 24, 48, and 72 h of SARS-CoV-2 infection. Uninfected cells at each time point (not shown) were set as 100% (control). (H) Western blots of infected Huh7 (lane 4), Huh7-RFP (lane 5), and Huh7-RFP-DCLK1 (lane 6) cells for expression of Spike and nucleocapsid proteins at 48 h.

to determine titers of live viral particles produced by infected cells. Huh7-RFP-DCLK1 cells increased the production of infectious viral particles by 4-fold at 48 h compared to controls (P = 0.002; Fig. 7F). With longer incubations (72 and 96 h postinfection), decreases in viral particles were most likely due to cell death (Fig. 7G) and reduced stability of viral particles in spent culture media. Others have reported significant losses of SARS-CoV-2 viability in liquid medium at 37 C within 1 to 2 days (44). Huh7-RFP-DCLK1 lysates showed increases in the large and S2 forms of Spike and nucleocapsid protein (p46) compared to controls (Fig. 7H) at 48 h, helping substantiate DCLK1-mediated

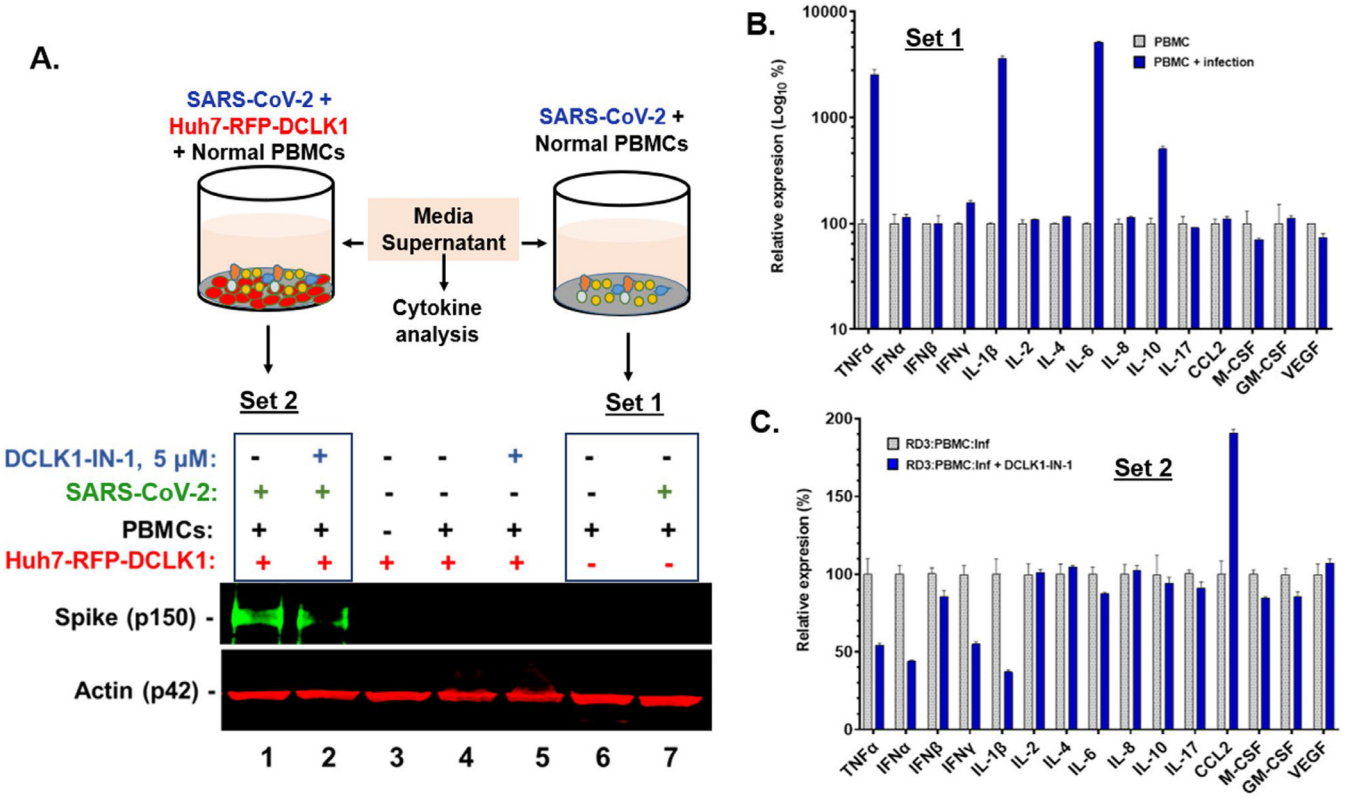

FIG 8 DCLK1-IN-1 inhibits viral replication and viral-induced inflammatory cytokines in DCLK1-overexpressing cells. (A) Mixed cocultures of normal human PBMCs with SARS-CoV-2-infected Huh7-RFP-DCLK1 cells were treated with 5 μM DCLK1-IN-1 (Set 2, lane 2) for 48 h. Similar untreated mixed cultures were used as a positive-control (lane 1) and other controls as indicated (Set 1, lanes 6 to 7). Culture lysates without infection show no Spike (lanes 3 to 7). Set 1, PBMC cultures (lane 6) were exposed to similar amounts of SARS-CoV-2 (lane 7) as in lanes 1 and 2. (B and C) Media supernatants of Set 2 and Set 1 cultures were assayed using the multiplexed cytokine assay kit. Marker expression in the untreated spent medium was calibrated at 100% and compared to inhibitor-treated samples in Set 2.

upregulation of viral production (Fig. 7F). These findings indicated that the increased expression of DCLK1 amplified SARS-CoV-2 production in liver cells.

Inhibition of DCLK1 kinase attenuated the SARS-CoV-2-induced cytokine signature. To assess the effect of DCLK1 kinase on cytokine production during SARS-CoV-2 infection, we mixed infected Huh7-RFP-DCLK1 cells with normal human PBMCs in the presence of 5 μM DCLK1-IN-1 for 48 h. Spent supernatants were assayed for cytokines/chemokines/growth factors using a multiplex system. As with infected Calu3 cells, DCLK1-IN-1 blocked Spike (Fig. 8A, lane 2, Set 2). Interestingly, PMBCs were not infected by SARS-CoV-2 and did not produce detectable Spike (Fig. 8A, lane 7, Set 1). However, PBMCs were responsive to SARS-CoV-2-infected cells as indicated by increased secretion of TNF-α, IL-1β, IL-6, and IL-10 in spent media compared to uninfected cells (Fig. 8B). DCLK1-IN-1 treatment led to downregulation of cytokines involved in inflammation and viral response (TNF-α, IFN-α, IFN-γ, and IL-1β; Fig. 8C). Interestingly, CCL2 (monocyte chemoattractant protein-1, MCP-1) was a noteworthy exception as this chemokine showed increased expression when infected cells were treated with DCLK1-IN-1. Because CCL2 participates in normal wound healing, an increase in this chemokine may contribute to tissue healing after viral clearance. In general, this *in vitro* system mimicked cytokine signatures observed in severe COVID-19 and the DCLK1 kinase inhibitor markedly attenuated this signature.

DISCUSSION

The progression of COVID-19 into severe/critical stages occurs more often in patients with underlying comorbidities, including chronic liver disease (CLD) (9, 45). Severe/critical SARS-CoV-2 infection is characterized by high levels of viral RNA in

plasma, hyperinflammation, and multiorgan failure that results in increased mortality (1, 46, 47). This study provides evidence that DCLK1 plays an important role in SARS-CoV-2 pathogenesis and immune dysregulation in COVID-19, especially for patients with CLD.

We found that DCLK1 was extensively expressed in the lungs and livers of individuals with COVID-19 who had underlying CLD. *In vitro*, DCLK1 increased viral particle production in lung and liver cells by 4 to 5-fold. A specific DCLK1 kinase inhibitor blunted viral production. This multifunctional kinase is known to modulate the cellular cytoskeleton by phosphorylating tubulin subunits (48). DCLK1 also autophosphorylates its C terminus at T688 residue to block hyperphosphorylation of N-terminal doublecortin domains. Hypophosphorylated and unphosphorylated doublecortin domains bind microtubules with higher affinity (49). Inhibition of T688 phosphorylation by DCLK1-IN-1 can disrupt DCLK1 interactions with microtubules and inhibition of the movement of viral RNA replication complexes. We previously observed the dynamic distribution of DCLK1-microtubule complexes in the filopodia of Huh7 cells by live cell imaging (unpublished data). It was recently reported that these protrusions in infected cells contain budding particles of SARS-CoV-2 (50). Additional work is needed, however, to better understand the mechanisms by which DCLK1 amplifies SARS-CoV-2 replication and trafficking within infected cells.

Our data further suggest the involvement of DCLK1 in a distinctive feed-forward signaling cascade with β-catenin, NF-κB, and S100A9 that can fuel inflammation and immune dysregulation in COVID-19 (12). We found that immune cells localized in alveolar and hepatic sinusoidal spaces in COVID-19 cases with CLD coexpressed DCLK1 and S100A9. Based on CD206 expression, these cells were consistent with M2-like macrophages. We also observed triple-positive DCLK1$^+$S100A9$^+$CD206$^+$ cells with segmented nuclei that likely represent N2-like neutrophils. Few DCLK1$^+$S100A9$^+$-expressing cells were observed in non-COVID-19 cases with chronic underlying lung disease or in normal controls (Table 1). In hospitalized patients with severe/critical COVID-19, these dually positive cells were detected in the blood. The SARS-CoV-2-dependent generation of these cells was substantiated using dual-chamber and mixed culture systems. These observations are consistent with prior reports showing high levels of calprotectin (a heterodimer of S100A8 and S100A9) in the blood of patients with severe COVID-19 (26, 28, 51). The M2- and N2-like phenotypes noted in autopsied COVID-19 cases would be expected to suppress antiviral innate immune responses, in part, through the upregulation of IL-10. Although DCLK1$^+$S100A9$^+$CD206$^+$ immune cells could be a potential marker for severe COVID-19, these findings require further study using a larger cohort of cases.

We found that DCLK1 facilitated the production of important inflammatory mediators *in vitro*. SARS-CoV-2-infected cells also induced GM-CSF, a chemoattractant that helps polarize macrophages toward an inflammatory M1-like phenotype. In our model, inhibiting DCLK1 kinase blocked inflammatory cytokines (IL-1β, IL-6, and TNF-α). Viral infection of liver cells also led to the induction of M-CSF and its receptor along with IL-10. IL-10 activates immunosuppressive immune cells (Th2) and helps polarize macrophages toward a CD206$^+$ M2 phenotype. The induction of the M1 phenotype would enhance inflammatory cytokine production while M2 phenotypes could facilitate higher levels of viremia by suppressing antiviral responses (Fig. 9). Our *in vitro* studies revealed that targeting both DCLK1 and S100A9 downregulated DCLK1 decreased β-catenin activation, and blocked caspase 1/IL-1β signaling. However, GM-CSF levels were not affected. In a clinical trial of lenzilumab, a GM-CSF inhibitor, the survival of COVID-19 patients was significantly improved (52). The potential combination of a DCLK1 kinase inhibitor with a GM-CSF inhibitor might further reduce viral replication and hyperinflammatory responses and improve outcomes.

DCLK1 and S100A9 are expressed in epithelial compartments of the liver following acute injury and with cirrhosis and hepatocellular carcinoma (12, 15, 21, 22). We noted strong expression of DCLK1 and S100A9 in livers of COVID-19 patients with CLD. Only weak, rare, or absent expression was noted in the livers of a normal case, or persons

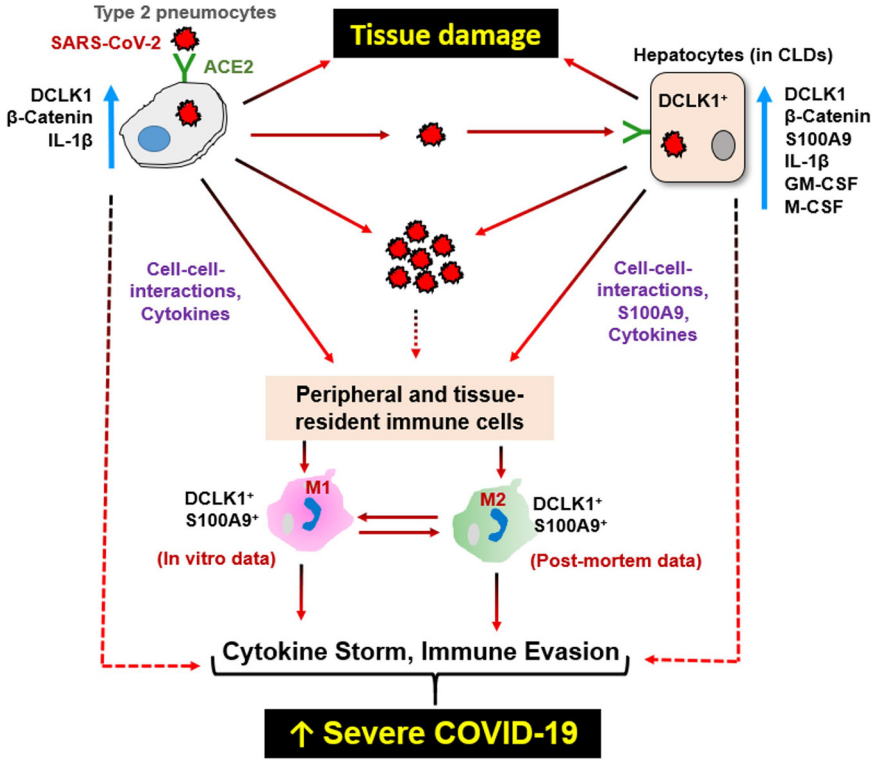

FIG 9 Potential mechanisms for DCLK1-regulated COVID-19 severity in patients with CLD. SARS-CoV-2 infection of Type II pneumocytes results in β-catenin(p65) activation (Fig. 5F) leading to the transcriptional activation of the DCLK1 (31). This results in the expression of the large isoform of DCLK1 mRNA, which can express the full-length protein (p82) or smaller isoforms by alternatively spliced mRNA or proteolytic cleavage of DCLK1(p82) (29–31). Viral infection of these cells also triggers DCLK1-dependent activation of inflammatory cytokines (TNF-α, IL-1β, and IFN-γ) (Fig. 5F and G and 8C). High-level expression of DCLK1 and S100A9 in CLD (12, 14, 21, 22) confers increased virus production and pathogenesis. Circulating viruses infect ACE2- and DCLK1-expressing hepatocytes in COVID-19 for individuals with CLD but not in individuals with healthy livers where these proteins are not expressed (Table 1). The infected pneumocytes and hepatocytes in CLD patients may produce additive or synergistic effects on viral load and inflammatory responses with the polarization of macrophages into proinflammatory M1 and immunosuppressive M2 (DCLK1+S100A9+CD206$^+$) phenotypes (Fig. 3) and by secreting cytokines and colony-stimulating factors (GM-CSF, MCSF) (Figs. 6B and 7C, D, and F). M2 macrophages produce IL-10 resulting in suppression of innate immunity. Mechanistically, DCLK1 upregulates S100A9 (12), which can bind to TLR4 and receptors for advanced glycation products to increase NF-κB signaling in immune cells (Fig. 6E) (27). DCLK1 upregulates S100A9 (12), which can bind to TLR4 and receptors for advanced glycation products to increase NF-κB signaling in immune cells (Fig. 6E) (27). Thus, additional investigations are needed to determine the interplay between these signaling molecules and whether a potential DCLK1/S100A9/NF-κB-mediated signaling process contributes to immune dysregulation in severe COVID-19.

without significant CLD (Table 1). We found evidence for robust SARS-CoV-2 infection only in livers with CLD. The expression of ACE2 on hepatocytes in CLD likely renders this organ susceptible to infection with SARS-CoV-2. Furthermore, our results suggest that DCLK1 expression in CLD amplifies SARS-CoV-2 replication. This might worsen viremia and disease severity in patients with COVID-19 and CLD.

In addition to viral production, DCLK1 may heighten inflammatory responses through β-catenin and DCLK1/S100A9/NF-κB signaling (12). This involves a feed-forward loop between S100A9 and NF-κB because DCLK1 and S100A9 each regulate the other's promoter (31, 35). Furthermore, S100A9 binds TLR4 and receptors for advanced glycation end products and could increase NF-κB signaling leading to NLRP3 activation in immune cells and the release of inflammatory cytokines (e.g., IL-1β and IL-6) by immune cells (27, 53). Indeed, SARS-CoV-2 infected cocultures of Calu3 and normal human PBMCs showed increased levels of p-NFκBp65^{Ser536} compared with uninfected controls (Fig. 4E). NLRP3 is activated in severe COVID-19 and may boost pro-IL-1β

processing. Thus, a DCLK1/S100A9/NF-κB feed-forward cycle could help drive persistent inflammatory responses and immune dysregulation. However, in hepatoma cells, we noted the downregulation of full-length NLRP3 following viral infection (Fig. 7E, lane 4) This led to the accumulation of procaspase 1 and pro-IL-1β. This agrees with reports by others where the translation of NSP1 and NSP13 proteins during the early phase of SARS-CoV-2 infection inhibits NLRP3 and IL-1β secretion (54). Inhibition of NLRP3 and IL-1β would be expected to facilitate viral propagation during early infection and promote immune evasion.

One limitation of this study was the lack of human leukocyte antigen (HLA) matching for normal PBMCs cultured with Huh7 and Calu3 cells. However, the coculture data were consistent with results obtained from flow cytometry analyses using PBMCs acquired from COVID-19 patients. In addition, cytokine changes were confirmed by loss-of-function and gain-of-function experiments. Another limitation involved the small number of autopsied individuals. Follow-up observations need to include larger cohorts. Finally, although an early strain of SARS-CoV-2 was used for these studies, we believe that DCLK1 and S100A9 represent host factors that would also likely be induced by recent emerging coronavirus variants and therefore should retain potential in the treatment of viral replication and hyperinflammation. In conclusion, our findings provide novel insights into the interplay between DCLK1 and SARS-CoV-2 infection in the context of CLD. DLCK1 is a host determinant that is expressed in CLD and as such represents a potential new target for therapy in this subset of patients with COVID-19. Small molecule inhibitors of DCLK1 kinase and S100A9/calprotectin simultaneously reduced viral production and inflammatory cytokines *in vitro* while impairing DCLK1 expression. Inhibiting DCLK1 kinase during SARS-CoV-2 infection may be an attractive new adjunct for the treatment of severe COVID-19.

MATERIALS AND METHODS

Collection of postmortem specimens, PBMCs, and sera from COVID-19 patients. Forensic pathologists performed complete postmortem examinations on cases brought to the Oklahoma City Office of the Chief Medical Examiner. The autopsies of individuals (n = 11) were performed following the recommended guidelines (33). The lungs and livers of these cases did not show evidence for autolysis by histological examination and were included in the study. For blood analysis of hospitalized COVID-19 patients (n = 18), PBMCs and corresponding sera were obtained from the Oklahoma Shared Clinical and Translation Resources (OSCTR) at Oklahoma University Health Sciences Center (OUHSC). Normal blood samples were donated by healthy adults and each tested negative for SARS-CoV-2 (n = 3). Normal PBMCs were purchased from ZenBio Inc. Infectious Diseases Society of America guidelines (https://www.idsociety.org) were used to classify COVID-19 cases as mild, moderate, and severe/critical. The study was approved by the Institutional Review Board (number 12906, dated 02/08/2021).

Cell cultures, SARS-CoV-2 infection, and $TCID_{50}$ assay. Lung adenocarcinoma cells (Calu-3, catalog number HTB-55) were purchased from ATCC. Hepatoma cells (Huh7), and derivative cells expressing recombinant fluorescent protein (Huh7-RFP) and RFP-DCLK1 (Huh7-RFP-DCLK1), have been previously described (12, 15). Cryopreserved primary human hepatocytes (Corning) and normal PBMCs (ZenBio) were purchased from vendors. All methods were carried out following the guidelines and regulations of the OUHSC Institutional Biosafety Committee (approval number 200470-2440A).

SARS-CoV-2 (USA-WA1/2020 strain) was obtained from BEI Resources at the National Institutes of Allergy and Infectious Diseases in Bethesda, Maryland (catalog number NR-52281). Coronavirus SARS-CoV-2 infectious clones, icSARS-CoV-2 were obtained from the World Reference Center for Emerging Viruses and Arboviruses through the University of Texas Medical Branch at Galveston, Texas. All experiments related to infectious clones and cultures were performed in a Biosafety Level-3 laboratory after Institutional Biosafety Committee approval (IBC Protocol number 100492). SARS-CoV-2 was grown for up to 3 passages in Vero-E6 cells (ATCC: CRL-1586) that were cultured in complete Dulbecco's Modified Eagle's Medium (DMEM) containing 5% fetal bovine serum (FBS) and antibiotics (Pen/Strep, Gibco), at 37°C and 5% CO_2. To passage SARS-CoV-2, Vero-E6 cells were grown in a T-150 flask to 50% confluence ($\sim$10 million cells) and inoculated with SARS-CoV-2 at a multiplicity of infection (MOI) of 0.001. Infections of cells were carried out in 3 mL of DMEM without FBS for 1 h at 37°C with gentle mixing. Cells were placed in complete media for 48 h. The virus was harvested from spent culture supernatants, centrifuged, and stored at $-$80°C. All experiments involving viral infection were conducted using viruses from the same stock. SARS-CoV-2 was titrated using the 50% tissue culture infectious dose ($TCID_{50}$) method (55). Vero-E6 cells were seeded at 10,000 cells per well in a 96-well plate, infected with serially diluted SARS-CoV-2 containing spent media, and cytopathic effects were determined after 96 h. The number of virus-positive wells was used to calculate a $TCID_{50}$/mL at each dilution.

SARS-CoV-2 infection of target cells in cocultures and evaluation of inhibitors. Huh7 cells, RFP- or RFP-DCLK1-expressing Huh7 cells, and Calu3 cells were infected for 2 h at 37°C with SARS-CoV-2

(multiplicity of infection = 1). Cell supernatants were collected at 24, 48, 72, and 96 h postinfection to detect productive virus infection. Viral titers in spent media were measured by $TCID_{50}$ (55). Huh7-RFP-DCLK1 cells were cultured in 6-well plates, infected for 2 h with SARS-COV-2 and DCLK1-IN-1 or DCLK1-NEG added at final concentrations of 0, 0.1, 2.5, 5.0, and 10 μM. The cells were lysed in RIPA buffer (Thermo Fisher), and total lysates were prepared using Bullet Blender's protocol (Next Advance, Inc.). Western blots were carried out with antibodies and fluorescence conjugated reagents and imaging was performed with the LI-COR imaging system. For coculture, purified PBMCs (10^6 per 6-well plate) from normal donors were added to cells 2 h postinfection. The effects of inhibitors were analyzed as above. Band intensities were calculated using Image Studio Digits. Images were produced in compliance with digital image and integrity policies.

Immunohistochemistry (IHC) and confocal microscopy. Deidentified lung and liver tissue slides were subjected to immunofluorescence staining using the Akoya Opal 7-Color IHC kit. Stained slides were imaged and evaluated by confocal microscopy (Leica SP8). The intensity of cellular staining was scored qualitatively by two investigators (NA and MMH) and a consensus was achieved. Staining was considered to be absent (−), rare (+/−), weak (+), moderate (++), or strong (+++). H&E-stained slides were used for pathological analyses. Fifty thousand PHHs from normal donors were cultured in a Lab-Teck II chambered system (Thermo Fisher) containing 100 μL Matrigel per well in Hepato-STIM hepatocyte defined medium supplemented with EGF (10 ng/mL). To perform confocal microscopy, cultures were fixed with 10% formamide-PBS for 20 m, blocked with 1% BSA in washing buffer (PBS, 0.5% Triton X-100, 0.05% Tween 20). After washing, the cells were stained with primary and secondary antibodies conjugated with fluorophores. Nuclear staining was carried out with 4′,6-diamidino-2-phenylindole (Dapi). Stained cells were subjected to confocal microscopy after the addition of ProLong Gold Anti-fade reagent (Invitrogen).

PBMC preparation, flow cytometry, and cytokine/chemokine analysis. PBMCs from COVID-19 patients were isolated using Lymphocyte Separation Medium (MediaTech/25-072-CV) and resuspended in CS10 solution at 1×10^6 cells/mL for cryopreservation. Frozen normal PBMCs were stained with Aqua-Zombie to determine live cells. Washed cells were fixed with 2% formaldehyde-PBS and permeabilized in 3.0% Triton X-100. Cells were treated with Fc blocker (BD 564220) in a mixture of Brilliant Stain Buffer (BD 563794) and eBioScience Flow Staining buffer (Invitrogen 00-4222-26). Cell staining was performed using antibody-fluorophore conjugates and, in parallel, with isotype IgG conjugates of corresponding fluorophores (BD Biosciences). Stained cells were subjected to data acquisition using a Stratedigm S1400Exi flow cytometer. Data were analyzed by FlowJo software. Compensation was performed using UltraComp eBeads Plus Compensation Beads (Invitrogen 01–3333-41) for each IgG-fluorochrome conjugate.

Tissue culture supernatants and sera were analyzed using a custom-made human Magnetic Luminex assay kit (LXSAHM-15; R&D Systems) for the following analytes: TNF-α, IFN-α, IFN-β, IFN-γ, IL-1β, IL-2, IL-4, IL-6, IL-8, IL-10, IL-17, CCL2, M-CSF, GM-CSF, and VEGF-A. Samples were processed in replicates and quantified using the BioPlex 200 System (Bio-Rad). The concentration of each analyte was expressed as pg/mg of total protein. Analyte levels in normal serum or control supernatants were set at 100% compared to test samples.

Statistical analysis. Statistical analyses were performed using Prism GraphPad software 9.0. Comparison between groups was made using a one-way analysis of variance (ANOVA). Multiple comparisons were done using the Šidák test with a single pooled variance. Cytokine/chemokine/growth factor data are presented as mean ± SEM. P values are expressed as: $P \geq 0.05$ (ns); $P < 0.05$ (*); $P < 0.01$ (**); $P < 0.001$ (***); and $P < 0.0001$ (****). A P value of 0.05 or lower was considered statistically significant.

Data availability. All data associated with this study are presented in the paper and supplemental materials. Materials will be available upon request.

SUPPLEMENTAL MATERIAL

Supplemental material is available online only.

SUPPLEMENTAL FILE 1, MP4 file, 6.9 MB.

SUPPLEMENTAL FILE 2, MP4 file, 6.9 MB.

SUPPLEMENTAL FILE 3, PDF file, 0.01 MB.

ACKNOWLEDGMENTS

Funding was provided by the National Institute of General Medical Sciences (P20GM103639) and the National Cancer Institute (R01-CA230641 to MMH and P30CA225520). This work was also supported by the OK-INBRE award to N.A. through the National Institute of General Medical Sciences of the National Institutes of Health under award P20GM103447. The content of this publication is solely the responsibility of the authors and does not necessarily represent the official views of the National Institutes of Health. Presbyterian Health Foundation (N.A.) and COMAA Research Fund Seed Grant (N.A.), and the Stephenson Cancer Center and Tobacco Settlement Endowment Trust (M.M.H.) also supported this work in part.

The OUHSC Laboratory for Molecular Biology and Cytometry Research provided flow cytometry and confocal microscopy services. Immunohistochemistry was performed by the Stephenson Cancer Center Pathology Core Laboratory. We thank Nathaniel S. Gray

(Stanford) for providing DCLK1-IN-1 and DCLK1-NEG and Ralf Janknetch for his careful review of the manuscript.

N.A. conceived the studies and devised and performed experiments; R.B.U., A.F., J.L.L., and N.A. performed experiments; M.M.H. and N.A., provided facilities, finalized data, devised experiments, and wrote the manuscript; J.C.H. helped in flow cytometry and confocal microscopy; S.A., performed IHC; E.S., L.M.B., and E.J.D. performed the autopsy and provided tissues; S.M. assisted with histologic evaluation; S.U., D.A., and C.W.H. contributed to the administrative support and discussed the data.

C.W.H. has an ownership interest with COARE Holdings, Inc. All remaining authors declare no competing interests.

REFERENCES

1. Merad M, Blish CA, Sallusto F, Iwasaki A. 2022. The immunology and immunopathology of COVID-19. Science 375:1122–1127. https://doi.org/10.1126/science.abm8108.
2. Konings F, Perkins MD, Kuhn JH, Pallen MJ, Alm EJ, Archer BN, Barakat A, Bedford T, Bhiman JN, Caly L, Carter LL, Cullinane A, de Oliveira T, Druce J, El Masry I, Evans R, Gao GF, Gorbalenya AE, Hamblion E, Herring BL, Hodcroft E, Holmes EC, Kakkar M, Khare S, Koopmans MPG, Korber B, Leite J, MacCannell D, Marklewitz M, Maurer-Stroh S, Rico JAM, Munster VJ, Neher R, Munnink BO, Pavlin BI, Peiris M, Poon L, Pybus O, Rambaut A, Resende P, Subissi L, Thiel V, Tong S, van der Werf S, von Gottberg A, Ziebuhr J, Van Kerkhove MD. 2021. SARS-CoV-2 variants of interest and concern naming scheme conducive for global discourse. Nat Microbiol 6:821–823. https://doi.org/10.1038/s41564-021-00932-w.
3. Zhou P, Yang XL, Wang XG, Hu B, Zhang L, Zhang W, Si HR, Zhu Y, Li B, Huang CL, Chen HD, Chen J, Luo Y, Guo H, Jiang RD, Liu MQ, Chen Y, Shen XR, Wang X, Zheng XS, Zhao K, Chen QJ, Deng F, Liu LL, Yan B, Zhan FX, Wang YY, Xiao GF, Shi ZL. 2020. A pneumonia outbreak associated with a new coronavirus of probable bat origin. Nature 579:270–273. https://doi.org/10.1038/s41586-020-2012-7.
4. Zhu N, Zhang D, Wang W, Li X, Yang B, Song J, Zhao X, Huang B, Shi W, Lu R, Niu P, Zhan F, Ma X, Wang D, Xu W, Wu G, Gao GF, Tan W. 2020. A novel coronavirus from patients with pneumonia in China. N Engl J Med 382:727–733. https://doi.org/10.1056/NEJMoa2001017.
5. Mathew D, Giles JR, Baxter AE, Oldridge DA, Greenplate AR, Wu JE, Alanio C, Kuri-Cervantes L, Pampena MB, D'Andrea K, Manne S, Chen Z, Huang YJ, Reilly JP, Weisman AR, Ittner CAG, Kuthuru O, Dougherty J, Nzingha K, Han N, Kim J, Pattekar A, Goodwin EC, Anderson EM, Weirick ME, Gouma S, Arevalo CP, Bolton MJ, Chen F, Lacey SF, Ramage H, Cherry S, Hensley SE, Apostolidis SA, Huang AC, Vella LA, Betts MR, Meyer NJ, Wherry EJ, Alam Z, Addison MM, Byrne KT, Chandra A, Descamps HC, Kaminskiy Y, Hamilton JT, Noll JH, Omran DK, Perkey E, Prager EM, The UPenn COVID Processing Unit, Betts MR, Meyer NJ, Wherry EJ. 2020. Deep immune profiling of COVID-19 patients reveals distinct immunotypes with therapeutic implications. Science 369:eabc8511. https://doi.org/10.1126/science.abc8511.
6. Tay MZ, Poh CM, Renia L, MacAry PA, Ng LFP. 2020. The trinity of COVID-19: immunity, inflammation and intervention. Nat Rev Immunol 20:363–374. https://doi.org/10.1038/s41577-020-0311-8.
7. Chu H, Chan JF, Yuen TT, Shuai H, Yuan S, Wang Y, Hu B, Yip CC, Tsang JO, Huang X, Chai Y, Yang D, Hou Y, Chik KK, Zhang X, Fung AY, Tsoi HW, Cai JP, Chan WM, Ip JD, Chu AW, Zhou J, Lung DC, Kok KH, To KK, Tsang OT, Chan KH, Yuen KY. 2020. Comparative tropism, replication kinetics, and cell damage profiling of SARS-CoV-2 and SARS-CoV with implications for clinical manifestations, transmissibility, and laboratory studies of COVID-19: an observational study. Lancet Microbe 1:e14–e23. https://doi.org/10.1016/S2666-5247(20)30004-5.
8. Moon AM, Webb GJ, Aloman C, Armstrong MJ, Cargill T, Dhanasekaran R, Genesca J, Gill US, James TW, Jones PD, Marshall A, Mells G, Perumalswami PV, Qi X, Su F, Ufere NN, Barnes E, Barritt AS, Marjot T. 2020. High mortality rates for SARS-CoV-2 infection in patients with pre-existing chronic liver disease and cirrhosis: preliminary results from an international registry. J Hepatol 73:705–708. https://doi.org/10.1016/j.jhep.2020.05.013.
9. Sarin SK, Choudhury A, Lau GK, Zheng MH, Ji D, Abd-Elsalam S, Hwang J, Qi X, Cua IH, Suh JI, Park JG, Putcharoen O, Kaewdech A, Piratvisuth T, Treeprasertsuk S, Park S, Wejnaruemarn S, Payawal DA, Baatarkhuu O, Ahn SH, Yeo CD, Alonzo UR, Chinbayar T, Loho IM, Yokosuka O, Jafri W, Tan S, Soo LI, Tanwandee T, Gani R, Anand L, Esmail ES, Khalaf M, Alam S, Lin CY, Chuang WL, Soin AS, Garg HK, Kalista K, Batsukh B, Purnomo HD, Dara VP, Rathi P, Al Mahtab M, Shukla A, Sharma MK, Omata M, Apasl Covid Task Force ACLISS. 2020. Pre-existing liver disease is associated with poor outcome in patients with SARS CoV2 infection; The APCOLIS Study (APASL COVID-19 Liver Injury Spectrum Study). Hepatol Int 14:690–700. https://doi.org/10.1007/s12072-020-10072-8.
10. Hamming I, Timens W, Bulthuis ML, Lely AT, Navis G, van Goor H. 2004. Tissue distribution of ACE2 protein, the functional receptor for SARS coronavirus. A first step in understanding SARS pathogenesis. J Pathol 203:631–637. https://doi.org/10.1002/path.1570.
11. Paizis G, Tikellis C, Cooper ME, Schembri JM, Lew RA, Smith AI, Shaw T, Warner FJ, Zuilli A, Burrell LM, Angus PW. 2005. Chronic liver injury in rats and humans upregulates the novel enzyme angiotensin converting enzyme 2. Gut 54:1790–1796. https://doi.org/10.1136/gut.2004.062398.
12. Ali N, Chandrakesan P, Nguyen CB, Husain S, Gillaspy AF, Huycke M, Berry WL, May R, Qu D, Weygant N, Sureban SM, Bronze MS, Dhanasekaran DN, Houchen CW. 2015. Inflammatory and oncogenic roles of a tumor stem cell marker doublecortin-like kinase (DCLK1) in virus-induced chronic liver diseases. Oncotarget 6:20327–20344. https://doi.org/10.18632/oncotarget.3972.
13. Nguyen CB, Kotturi H, Waris G, Mohammed A, Chandrakesan P, May R, Sureban S, Weygant N, Qu D, Rao CV, Dhanasekaran DN, Bronze MS, Houchen CW, Ali N. 2016. (Z)-3,5,4'-trimethoxystilbene limits hepatitis C and cancer pathophysiology by blocking microtubule dynamics and cell-cycle progression. Cancer Res 76:4887–4896. https://doi.org/10.1158/0008-5472.CAN-15-2722.
14. Fan M, Qian N, Dai G. 2017. Expression and prognostic significance of doublecortin-like kinase 1 in patients with hepatocellular carcinoma. Oncology Lett 14:7529–7537. https://doi.org/10.3892/ol.2017.7082.
15. Ali N, Nguyen CB, Chandrakesan P, Wolf RF, Qu D, May R, Goretsky T, Fazili J, Barrett TA, Li M, Huycke MM, Bronze MS, Houchen CW. 2020. Doublecortin-like kinase 1 promotes hepatocyte clonogenicity and oncogenic programming via non-canonical b-catenin-dependent mechanism. Sci Rep 10:10578. https://doi.org/10.1038/s41598-020-67401-y.
16. Westphalen CB, Asfaha S, Hayakawa Y, Takemoto Y, Lukin DJ, Nuber AH, Brandtner A, Setlik W, Remotti H, Muley A, Chen X, May R, Houchen CW, Fox JG, Gershon MD, Quante M, Wang TC. 2014. Long-lived intestinal tuft cells serve as colon cancer-initiating cells. J Clin Invest 124:1283–1295. https://doi.org/10.1172/JCI73434.
17. Chandrakesan P, Weygant N, May R, Qu D, Chinthalapally HR, Sureban SM, Ali N, Lightfoot SA, Umar S, Houchen CW. 2014. DCLK1 facilitates intestinal tumor growth via enhancing pluripotency and epithelial mesenchymal transition. Oncotarget 5:9269–9280. https://doi.org/10.18632/oncotarget.2393.
18. Nakanishi Y, Seno H, Fukuoka A, Ueo T, Yamaga Y, Maruno T, Nakanishi N, Kanda K, Komekado H, Kawada M, Isomura A, Kawada K, Sakai Y, Yanagita M, Kageyama R, Kawaguchi Y, Taketo MM, Yonehara S, Chiba T. 2013. Dclk1 distinguishes between tumor and normal stem cells in the intestine. Nat Genet 45:98–103. https://doi.org/10.1038/ng.2481.
19. Greber UF, Way M. 2006. A superhighway to virus infection. Cell 124:741–754. https://doi.org/10.1016/j.cell.2006.02.018.
20. Liu Y, Ferguson FM, Li L, Kuljanin M, Mills CE, Subramanian K, Harshbarger W, Gondi S, Wang J, Sorger PK, Mancias JD, Gray NS, Westover KD. 2020. Chemical biology toolkit for DCLK1 reveals connection to RNA processing. Cell Chem Biol 27:1229–1240.e4. https://doi.org/10.1016/j.chembiol.2020.07.011.
21. Ali N, Allam H, Bader T, May R, Basalingappa KM, Berry WL, Chandrakesan P, Qu D, Weygant N, Bronze MS, Umar S, Janknecht R, Sureban SM, Huycke M,

Houchen CW. 2013. Fluvastatin interferes with hepatitis C virus replication via microtubule bundling and a doublecortin-like kinase-mediated mechanism. PLoS One 8:e80304. https://doi.org/10.1371/journal.pone.0080304.
22. Ali N, Allam H, May R, Sureban SM, Bronze MS, Bader T, Umar S, Anant S, Houchen CW. 2011. Hepatitis C virus-induced cancer stem cell-like signatures in cell culture and murine tumor xenografts. J Virol 85:12292–12303. https://doi.org/10.1128/JVI.05920-11.
23. Sureban SM, Madhoun MF, May R, Qu D, Ali N, Fazili J, Weygant N, Chandrakesan P, Ding K, Lightfoot SA, Houchen CW. 2015. Plasma DCLK1 is a marker of hepatocellular carcinoma (HCC): targeting DCLK1 prevents HCC tumor xenograft growth via a microRNA-dependent mechanism. Oncotarget 6:37200–37215. https://doi.org/10.18632/oncotarget.5808.
24. Tardif JC, Bouabdallaoui N, L'Allier PL, Gaudet D, Shah B, Pillinger MH, Lopez-Sendon J, da Luz P, Verret L, Audet S, Dupuis J, Denault A, Pelletier M, Tessier PA, Samson S, Fortin D, Tardif JD, Busseuil D, Goulet E, Lacoste C, Dubois A, Joshi AY, Waters DD, Hsue P, Lepor NE, Lesage F, Sainturet N, Roy-Clavel E, Bassevitch Z, Orfanos A, Stamatescu G, Gregoire JC, Busque L, Lavallee C, Hetu PO, Paquette JS, Deftereos SG, Levesque S, Cossette M, Nozza A, Chabot-Blanchet M, Dube MP, Guertin MC, Boivin G, Investigators C. 2021. Colchicine for community-treated patients with COVID-19 (COLCORONA): a phase 3, randomised, double-blinded, adaptive, placebo-controlled, multicentre trial. Lancet Respir Med 9:924–932. https://doi.org/10.1016/S2213-2600(21)00222-8.
25. Vogl T, Gharibyan AL, Morozova-Roche LA. 2012. Pro-inflammatory S100A8 and S100A9 proteins: self-assembly into multifunctional native and amyloid complexes. Int J Mol Sci 13:2893–2917. https://doi.org/10.3390/ijms13032893.
26. Mahler M, Meroni PL, Infantino M, Buhler KA, Fritzler MJ. 2021. Circulating Calprotectin as a Biomarker of COVID-19 Severity. Expert Rev Clin Immunol 17:431–443. https://doi.org/10.1080/1744666X.2021.1905526.
27. Simard JC, Cesaro A, Chapeton-Montes J, Tardif M, Antoine F, Girard D, Tessier PA. 2013. S100A8 and S100A9 induce cytokine expression and regulate the NLRP3 inflammasome via ROS-dependent activation of NF-kappaB(1.). PLoS One 8:e72138. https://doi.org/10.1371/journal.pone.0072138.
28. Guo Q, Zhao Y, Li J, Liu J, Yang X, Guo X, Kuang M, Xia H, Zhang Z, Cao L, Luo Y, Bao L, Wang X, Wei X, Deng W, Wang N, Chen L, Chen J, Zhu H, Gao R, Qin C, Wang X, You F. 2021. Induction of alarmin S100A8/A9 mediates activation of aberrant neutrophils in the pathogenesis of COVID-19. Cell Host Microbe 29:222–235.e4. https://doi.org/10.1016/j.chom.2020.12.016.
29. Burgess HA, Reiner O. 2001. Cleavage of doublecortin-like kinase by calpain releases an active kinase fragment from a microtubule anchorage domain. J Biol Chem 276:36397–36403. https://doi.org/10.1074/jbc.M105153200.
30. Burgess HA, Reiner O. 2002. Alternative splice variants of doublecortin-like kinase are differentially expressed and have different kinase activities. J Biol Chem 277:17696–17705. https://doi.org/10.1074/jbc.M111981200.
31. O'Connell MR, Sarkar S, Luthra GK, Okugawa Y, Toiyama Y, Gajjar AH, Qiu S, Goel A, Singh P. 2015. Epigenetic changes and alternate promoter usage by human colon cancers for expressing DCLK1-isoforms: clinical Implications. Sci Rep 5:14983. https://doi.org/10.1038/srep14983.
32. Liu X, Wang Y, Ming Y, Song Y, Zhang J, Chen X, Zeng M, Mao Y. 2015. S100A9: a potential biomarker for the progression of non-alcoholic fatty liver disease and the diagnosis of non-alcoholic steatohepatitis. PLoS One 10:e0127352. https://doi.org/10.1371/journal.pone.0127352.
33. Barton LM, Duval EJ, Stroberg E, Ghosh S, Mukhopadhyay S. 2020. COVID-19 Autopsies, Oklahoma, USA. Am J Clin Pathol 153:725–733. https://doi.org/10.1093/ajcp/aqaa062.
34. Huang M, Wu R, Chen L, Peng Q, Li S, Zhang Y, Zhou L, Duan L. 2019. S100A9 regulates MDSCs-mediated immune suppression via the RAGE and TLR4 signaling pathways in colorectal carcinoma. Front Immunol 10:2243. https://doi.org/10.3389/fimmu.2019.02243.
35. Nemeth J, Stein I, Haag D, Riehl A, Longerich T, Horwitz E, Breuhahn K, Gebhardt C, Schirmacher P, Hahn M, Ben-Neriah Y, Pikarsky E, Angel P, Hess J. 2009. S100A8 and S100A9 are novel nuclear factor kappa B target genes during malignant progression of murine and human liver carcinogenesis. Hepatology 50:1251–1262. https://doi.org/10.1002/hep.23099.
36. Puhl SL, Steffens S. 2019. Neutrophils in post-myocardial infarction inflammation: damage vs. resolution? Front Cardiovasc Med 6:25. https://doi.org/10.3389/fcvm.2019.00025.
37. Ferguson FM, Nabet B, Raghavan S, Liu Y, Leggett AL, Kuljanin M, Kalekar RL, Yang A, He S, Wang J, Ng RWS, Sulahian R, Li L, Poulin EJ, Huang L, Koren J, Dieguez-Martinez N, Espinosa S, Zeng Z, Corona CR, Vasta JD, Ohi R, Sim T, Kim ND, Harshbarger W, Lizcano JM, Robers MB, Muthaswamy S, Lin CY, Look AT, Haigis KM, Mancias JD, Wolpin BM, Aguirre AJ, Hahn WC, Westover KD, Gray NS. 2020. Discovery of a selective inhibitor of doublecortin like kinase 1. Nat Chem Biol 16:635–643. https://doi.org/10.1038/s41589-020-0506-0.
38. van Noort M, Meeldijk J, van der Zee R, Destree O, Clevers H. 2002. Wnt signaling controls the phosphorylation status of b-catenin. J Biol Chem 277:17901–17905. https://doi.org/10.1074/jbc.M111635200.
39. Jontvedt Jorgensen M, Holter JC, Christensen EE, Schjalm C, Tonby K, Pischke SE, Jenum S, Skeie LG, Nur S, Lind A, Opsand H, Enersen TB, Grondahl R, Hermann A, Dudman S, Muller F, Ueland T, Mollnes TE, Aukrust P, Heggelund L, Holten AR, Dyrhol-Riise AM. 2020. Increased interleukin-6 and macrophage chemoattractant protein-1 are associated with respiratory failure in COVID-19. Sci Rep 10:21697. https://doi.org/10.1038/s41598-020-78710-7.
40. Chen Y, Wang J, Liu C, Su L, Zhang D, Fan J, Yang Y, Xiao M, Xie J, Xu Y, Li Y, Zhang S. 2020. IP-10 and MCP-1 as biomarkers associated with disease severity of COVID-19. Mol Med 26:97. https://doi.org/10.1186/s10020-020-00230-x.
41. Riva M, Kallberg E, Bjork P, Hancz D, Vogl T, Roth J, Ivars F, Leanderson T. 2012. Induction of nuclear factor-kappaB responses by the S100A9 protein is Toll-like receptor-4-dependent. Immunology 137:172–182. https://doi.org/10.1111/j.1365-2567.2012.03619.x.
42. Del Valle DM, Kim-Schulze S, Huang HH, Beckmann ND, Nirenberg S, Wang B, Lavin Y, Swartz TH, Madduri D, Stock A, Marron TU, Xie H, Patel M, Tuballes K, Van Oekelen O, Rahman A, Kovatch P, Aberg JA, Schadt E, Jagannath S, Mazumdar M, Charney AW, Firpo-Betancourt A, Mendu DR, Jhang J, Reich D, Sigel K, Cordon-Cardo C, Feldmann M, Parekh S, Merad M, Gnjatic S. 2020. An inflammatory cytokine signature predicts COVID-19 severity and survival. Nat Med 26:1636–1643. https://doi.org/10.1038/s41591-020-1051-9.
43. Appelberg S, Gupta S, Svensson Akusjarvi S, Ambikan AT, Mikaeloff F, Saccon E, Vegvari A, Benfeitas R, Sperk M, Stahlberg M, Krishnan S, Singh K, Penninger JM, Mirazimi A, Neogi U. 2020. Dysregulation in Akt/mTOR/HIF-1 signaling identified by proteo-transcriptomics of SARS-CoV-2 infected cells. Emerg Microbes Infect 9:1748–1760. https://doi.org/10.1080/22221751.2020.1799723.
44. Chan KH, Sridhar S, Zhang RR, Chu H, Fung AY, Chan G, Chan JF, To KK, Hung IF, Cheng VC, Yuen KY. 2020. Factors affecting stability and infectivity of SARS-CoV-2. J Hosp Infect 106:226–231. https://doi.org/10.1016/j.jhin.2020.07.009.
45. Marjot T, Moon AM, Cook JA, Abd-Elsalam S, Aloman C, Armstrong MJ, Pose E, Brenner EJ, Cargill T, Catana MA, Dhanasekaran R, Eshraghian A, Garcia-Juarez I, Gill US, Jones PD, Kennedy J, Marshall A, Matthews C, Mells G, Mercer C, Perumalswami PV, Avitabile E, Qi X, Su F, Ufere NN, Wong YJ, Zheng MH, Barnes E, Barritt A, Webb GJ. 2021. Outcomes following SARS-CoV-2 infection in patients with chronic liver disease: an international registry study. J Hepatol 74:567–577. https://doi.org/10.1016/j.jhep.2020.09.024.
46. Nalbandian A, Sehgal K, Gupta A, Madhavan MV, McGroder C, Stevens JS, Cook JR, Nordvig AS, Shalev D, Sehrawat TS, Ahluwalia N, Bikdeli B, Dietz D, Der-Nigoghossian C, Liyanage-Don N, Rosner GF, Bernstein EJ, Mohan S, Beckley AA, Seres DS, Choueiri TK, Uriel N, Ausiello JC, Accili D, Freedberg DE, Baldwin M, Schwartz A, Brodie D, Garcia CK, Elkind MSV, Connors JM, Bilezikian JP, Landry DW, Wan EY. 2021. Post-acute COVID-19 syndrome. Nat Med 27:601–615. https://doi.org/10.1038/s41591-021-01283-z.
47. Fajnzylber J, Regan J, Coxen K, Corry H, Wong C, Rosenthal A, Worrall D, Giguel F, Piechocka-Trocha A, Atyeo C, Fischinger S, Chan A, Flaherty KT, Hall K, Dougan M, Ryan ET, Gillespie E, Chishti R, Li Y, Jilg N, Hanidziar D, Baron RM, Baden L, Tsibris AM, Armstrong KA, Kuritzkes DR, Alter G, Walker BD, Yu X, Li JZ, Massachusetts Consortium for Pathogen R. 2020. SARS-CoV-2 viral load is associated with increased disease severity and mortality. Nat Commun 11:5493. https://doi.org/10.1038/s41467-020-19057-5.
48. Koizumi H, Fujioka H, Togashi K, Thompson J, Yates JR, 3rd, Gleeson JG, Emoto K. 2017. DCLK1 phosphorylates the microtubule-associated protein MAP7D1 to promote axon elongation in cortical neurons. Dev Neurobiol 77:493–510. https://doi.org/10.1002/dneu.22428.
49. Agulto RL, Rogers MM, Tan TC, Ramkumar A, Downing AM, Bodin H, Castro J, Nowakowski DW, Ori-McKenney KM. 2021. Autoregulatory control of microtubule binding in doublecortin-like kinase 1. Elife 10:e60126. https://doi.org/10.7554/eLife.60126.
50. Bouhaddou M, Memon D, Meyer B, White KM, Rezelj VV, Correa Marrero M, Polacco BJ, Melnyk JE, Ulferts S, Kaake RM, Batra J, Richards AL, Stevenson E, Gordon DE, Rojc A, Obernier K, Fabius JM, Soucheray M, Miorin L, Moreno E, Koh C, Tran QD, Hardy A, Robinot R, Vallet T, Nilsson-Payant BE, Hernandez-Armenta C, Dunham A, Weigang S, Knerr J, Modak M, Quintero D, Zhou Y, Dugourd A, Valdeolivas A, Patil T, Li Q, Hüttenhain

R, Cakir M, Muralidharan M, Kim M, Jang G, Tutuncuoglu B, Hiatt J, Guo JZ, Xu J, Bouhaddou S, Mathy CJP, Gaulton A, Manners EJ, et al. 2020. The global phosphorylation landscape of SARS-CoV-2 infection. Cell 182:685–712.e19. https://doi.org/10.1016/j.cell.2020.06.034.

51. Silvin A, Chapuis N, Dunsmore G, Goubet AG, Dubuisson A, Derosa L, Almire C, Henon C, Kosmider O, Droin N, Rameau P, Catelain C, Alfaro A, Dussiau C, Friedrich C, Sourdeau E, Marin N, Szwebel TA, Cantin D, Mouthon L, Borderie D, Deloger M, Bredel D, Mouraud S, Drubay D, Andrieu M, Lhonneur AS, Saada V, Stoclin A, Willekens C, Pommeret F, Griscelli F, Ng LG, Zhang Z, Bost P, Amit I, Barlesi F, Marabelle A, Pene F, Gachot B, Andre F, Zitvogel L, Ginhoux F, Fontenay M, Solary E. 2020. Elevated calprotectin and abnormal myeloid cell subsets discriminate severe from mild COVID-19. Cell 182:1401–1418.e18. https://doi.org/10.1016/j.cell.2020.08.002.
52. Temesgen Z, Burger CD, Baker J, Polk C, Libertin CR, Kelley CF, Marconi VC, Orenstein R, Catterson VM, Aronstein WS, Durrant C, Chappell D, Ahmed O, Chappell G, Badley AD, Lewis M, Sher L, Bowdish M, Wald-Dickler N, Biswas S, Lam L, Vo K, Poblete R, Lee MM, Hutcheon D, Patron R, Gharbin J, Moran C, Kandiah S, Cantos V, Rebolledo P, del Rio C, Lennox J, Polito C, Sheth A, Patel A, Paniagua H, Yohannes S, Amin A, Lee R, Watanabe M, Hsieh L, Cearras M, Parikh A, Sniffen J, Onyia W, Boger M, Davidson L, Gajurel K, Leonard M, Group L-AS. 2022. Lenzilumab in hospitalised patients with COVID-19 pneumonia (LIVE-AIR): a phase 3, randomised, placebo-controlled trial. Lancet Respir Med 10:237–246. https://doi.org/10.1016/S2213-2600(21)00494-X.
53. Sternberg C, Armstrong A, Pili R, Ng S, Huddart R, Agarwal N, Khvorostenko D, Lyulko O, Brize A, Vogelzang N, Delva R, Harza M, Thanos A, James N, Werbrouck P, Bogemann M, Hutson T, Milecki P, Chowdhury S, Gallardo E, Schwartsmann G, Pouget JC, Baton F, Nederman T, Tuvesson H, Carducci M. 2016. Randomized, double-blind, placebo-controlled phase III study of tasquinimod in men with metastatic castration-resistant prostate cancer. JCO 34:2636–2643. https://doi.org/10.1200/JCO.2016.66.9697.
54. Kim NE, Kim DK, Song YJ. 2021. SARS-CoV-2 nonstructural proteins 1 and 13 suppress caspase-1 and the NLRP3 inflammasome activation. Microorganisms 9:494. https://doi.org/10.3390/microorganisms9030494.
55. Reed LJ. 1938. A simple method of estimating fifty per cent endpoints. Am J Hyg 27:493–497.